

1

2

3 **Preservation of KCC2 expression in axotomized abducens**
4 **motoneurons and its enhancement by VEGF**

3

4 Paula M. Calvo^{1,2}, Rosa R. de la Cruz¹, Angel M. Pastor^{1*} and Francisco J. Alvarez^{2*#}

5

6

7 ¹Departamento de Fisiología, Facultad de Biología, Universidad de Sevilla,
8 41012-Sevilla, Spain and ²Department of Cell Biology, Emory University, Atlanta, GA
9 30322

10

11 (*) A.M.P. and F.J.A. are co-senior authors

12

13 **(#) Corresponding author:**

14 Dr. Francisco J. Alvarez
15 Emory University
16 Atlanta, GA 30322
17 e-mail: francisco.j.alvarez@emory.edu

18

19 **Paula M Calvo** ORCID: 0000-0001-9817-8728

20 **Rosa R de la Cruz** ORCID: 0000-0001-5301-5108

21 **Angel M. Pastor** ORCID: 0000-0002-6213-7454

22 **Francisco J. Alvarez** ORCID: 0000-0001-7011-3244

23

24 **Acknowledgments:**

25 **Funding:** This work was funded by NIH (NINDS) R01 NS111969 and R21 NS114839
26 to F.J.A. This publication is also part of the I+D+i project P20_00529 Consejería de
27 Transformación Económica Industria y Conocimiento, Junta de Andalucía-FEDER.
28 Research materials were also supported by project PGC2018-094654-B-100 and
29 PID2021-124300NB-I00 both funded by MCIN/AEI/FEDER “A way of making Europe”
30 to A.M.P and R.R.C. P.M.C. was a scholar of Ministerio de Educación y Ciencia (BES-

31 2016-077912) in Spain and now a “Margarita Salas” postdoctoral fellow from Spain at
32 Emory University Atlanta, USA.

33

34 **Abstract**

35 The potassium chloride cotransporter 2 (KCC2) is the main Cl⁻ extruder in neurons. Any
36 alteration in KCC2 levels leads to changes in Cl⁻ homeostasis and, consequently, in the
37 polarity and amplitude of inhibitory synaptic potentials mediated by GABA or glycine.
38 Axotomy downregulates KCC2 in many different motoneurons and it is suspected that
39 interruption of muscle-derived factors maintaining motoneuron KCC2 expression is in
40 part responsible. In here, we demonstrate that KCC2 is expressed in all oculomotor nuclei
41 of cat and rat, but while trochlear and oculomotor motoneurons downregulate KCC2 after
42 axotomy, expression is unaltered in abducens motoneurons. Exogenous application of
43 vascular endothelial growth factor (VEGF), a neurotrophic factor expressed in muscle,
44 upregulated KCC2 in axotomized abducens motoneurons above control levels. In parallel,
45 a physiological study using cats chronically implanted with electrodes for recording
46 abducens motoneurons in awake animals, demonstrated that inhibitory inputs related to
47 off-fixations and off-directed saccades in VEGF-treated axotomized abducens
48 motoneurons were significantly higher than in control, but eye-related excitatory signals
49 in the on direction were unchanged. This is the first report of lack of KCC2 regulation in
50 a motoneuron type after injury, proposing a role for VEGF in KCC2 regulation and
51 demonstrating the link between KCC2 and synaptic inhibition in awake, behaving
52 animals.

53

54 **Keywords:** oculomotor system, inhibitory synapses, neurotrophic factors, eye
55 movements, vestibular

56

57

58 **Introduction**

59 The K^+/Cl^- cotransporter 2 (KCC2) is the main extruder of Cl^- in neurons (Payne et al.
60 1996, 2003; Chamma et al. 2012; Kaila et al. 2014) and plays critical roles in Cl^-
61 homeostasis and in maintaining the excitatory/inhibitory synaptic balance. Thus,
62 increases in KCC2 produce inhibitory postsynaptic potentials of higher amplitude in
63 response to the inhibitory neurotransmitters GABA or glycine. A decrease in KCC2 leads
64 to Cl^- accumulation inside neurons, making the Cl^- equilibrium potential less negative
65 resulting in weaker inhibition or even depolarizing postsynaptic potentials (Chamma et
66 al. 2012; Medina et al. 2014; Côme et al. 2019). GABA depolarizing actions during early
67 development, when KCC2 levels in neurons are low, are well known and KCC2 posterior
68 upregulation contributes to render GABA and glycine into inhibitory neurotransmitters
69 (Rivera et al. 1999; Zhu et al. 2008; Ben-Ari 2014; Peerboom and Wierenga 2021). In the
70 adult, low levels of KCC2 are associated with pathologies characterized by
71 hyperexcitability such as epilepsy, spasticity, neuropathic pain, ischemia, spinal cord
72 injury or schizophrenia (Beverungen et al. 2002; Woo et al. 2002; Palma et al. 2006;
73 Cramer et al. 2008; Papp et al. 2008; Boulenguez et al. 2010; Akita and Fukuda 2020;
74 Pozzi et al. 2020), while KCC2 enhancement ameliorates dysfunction (Gagnon et al.
75 2013; Kahle et al. 2014; Moore et al. 2018; Lorenzo et al. 2020; Bilchack et al. 2021).

76 Axotomy of spinal, facial, hypoglossal and dorsal vagus motoneurons also induces
77 rapid downregulation of *kcc2* gene expression followed by decreased KCC2 protein
78 levels on the membrane (Nabekura et al. 2002; Toyoda et al. 2003; Tatetsu et al. 2012;
79 Kim et al. 2018; Akhter et al. 2019). KCC2 downregulation in axotomized motoneurons
80 causes an increase in internal Cl^- that results in GABA-induced depolarizing oscillations
81 (Toyoda et al. 2003) resembling those found in immature neurons. Consequently,
82 inhibitory drive is absent and GABAergic/glycinergic synapses depolarize axotomized

83 motoneurons. When regeneration is allowed, KCC2 levels return to normal after motor
84 axons reinnervate muscles (Tatetsu et al. 2012; Kim et al. 2018; Akhter et al. 2019),
85 suggesting that target-derived factors are important regulators of KCC2 in motoneurons.
86 Surprisingly, despite extensive literature linking BDNF/TrkB signaling with KCC2
87 regulation (Rivera et al. 2002; Aguado et al. 2003; Rivera et al. 2004; Miletic and Miletic
88 2008; Boulenguez et al. 2010; Ludwig et al. 2011), axotomized motoneurons regulate
89 KCC2 expression independent of BDNF (Akhter et al. 2019) by mechanisms currently
90 unknown.

91 KCC2 regulation in axotomized extraocular motoneurons, a type of motoneuron
92 particularly resilient to certain types of injuries, is yet unexplored. Extensive studies
93 performed in cats chronically implanted with electrodes to monitor motoneuron function
94 in awake unanesthetized animals have shown that axotomy of abducens motoneurons
95 results in many physiological and synaptic changes that are responsive to a variety of
96 trophic factors (reviewed in Benitez-Temiño et al. 2016). Recently, we found that
97 vascular endothelial growth factor (VEGF) was the most effective neurotrophic factor in
98 maintaining normal synaptic function on axotomized abducens motoneurons (Calvo et al.
99 2018, 2020). This agrees with previous research on VEGF significance for survival and
100 maintenance of the morpho-physiological phenotype of injured motoneurons (Oosthuysen
101 et al. 2001; Azzouz et al. 2004; Tovar-y-Romo et al. 2007). Thus, we hypothesized that
102 i) VEGF could be a muscle-derived trophic factor; ii) axotomy should downregulate
103 KCC2 in abducens motoneurons and that iii) exogenously-supplied VEGF after axotomy
104 prevents KCC2 downregulation. .

105 The results surprisingly showed that axotomy did not downregulate KCC2 in
106 abducens motoneurons. Further studies across species and in different motoneuron types
107 demonstrated the uniqueness of this absence of regulation in abducens motoneurons.

108 Interestingly, VEGF upregulated KCC2 in axotomized abducens motoneurons above
109 control levels and this correlated with a potentiation of inhibition in these injured
110 motoneurons. The results thus suggest that abducens motoneurons and VEGF are
111 valuable models to test mechanisms that preserve KCC2 expression and inhibition in
112 injured neurons.

11311
3

114 **Materials and Methods**

115 **Animals and surgical procedures**

116 Experiments were performed on 12 adult female cats weighing 2.0-2.5 kg obtained from
117 an authorized supplier (Universidad de Córdoba, Spain), and 3 adult rats obtained from
118 our animal facilities (Biology School, University of Sevilla, Spain) (Table 1 for details).
119 Out of the 12 cats, 9 belonged to two previous studies: 7 from Calvo et al., 2018, and 2
120 from Calvo et al., 2020, and provided data for the abducens study. The last 3 cats were
121 used for tibial nerve axotomy.

122 Abducens nerve axotomy is described in detail in Calvo et al. 2018. Briefly, the
123 left VIth nerve was sectioned at its entry into the lateral rectus muscle and the lateral
124 rectus muscle removed. A custom-made chamber was placed by suction in the proximal
125 stump of the severed nerve to prevent reinnervation (i.e., the intraorbital device). VEGF
126 was administered in axotomized animals through the proximal stump of the (left) VIth
127 sectioned nerve (Calvo et al. 2018). Control data for testing KCC2 levels were obtained
128 from the control side of axotomized or axotomized + VEGF-treated animals (Table 1).

129 For the electrophysiological analyses, the firing behavior of abducens
130 motoneurons was recorded sequentially in two animals first in control, then after axotomy
131 and finally after axotomy + VEGF treatment. Control recordings were also obtained from
132 two additional animals (Calvo et al. 2018, 2020; Table 1). In all cases, animals were

133 euthanized under deep terminal anesthesia (sodium pentobarbital, 100 mg/kg, i.p.) and
 134 transcardially perfused with physiological saline followed by fixative consisting of 4%
 135 paraformaldehyde prepared in 0.1 M sodium phosphate buffer (PB), pH 7.4. The
 136 brainstems were collected and the abducens region cut at 50 μ m thickness using a
 137 vibratome.

Animal #	Surgery	Treatment	Survival (days)	Chronic recordings
Cat 1-4	Left VIth nerve cut	Axotomy+VEGF	20+20	Yes
Cat 5-6	Left VIth nerve cut	Axotomy+VEGF	20+20	No
Cat 7-9	Left VIth nerve cut	Axotomy	20-21	No
Cat 10-12	Left tibial nerve cut	Axotomy	21	No
Rat 1-3	Left eye enucleation & facial nerve cut	Axotomy	15	No

138 **Table 1** Animals used in this study

139139

140 To compare the effects of axotomy on KCC2 levels between cat abducens and
 141 spinal motoneurons three further cats were prepared for the tibial nerve axotomy. Thus,
 142 under general anesthesia (ketamine hydrochloride 20 mg/kg mixed with xylazine 0.5
 143 mg/kg, i.m.), the left tibial nerve was sectioned, and a ligature was made to the proximal
 144 stump of the nerve to prevent regeneration. Then, the incision made in the skin was
 145 surgically sutured and the animals were allowed to recover. After 21 days the animals
 146 were perfusion-fixed as described above and the lumbar spinal cord was extracted and
 147 cut at 50 μ m thick coronal sections on a vibratome.

148 To test for any possible species differences, we also studied the response of KCC2
 149 to axotomy in all extraocular motoneurons, as well as in facial motoneurons in rats. Non-
 150 extraocular cranial motoneurons have been reported to downregulate KCC2 levels after
 151 axotomy in rodents, including those of the vagus dorsal motor nucleus, and hypoglossal
 152 and facial motoneurons (Nabekura et al. 2002; Tatetsu et al. 2012; Kim et al. 2018), but
 153 no work has reported to date the effects of axotomy on KCC2 levels in the extraocular
 154 motoneurons in rats. We operated 3 adult Wistar rats. Under general anesthesia (sodium

155 pentobarbital, 35 mg/kg, i.p.), animals were unilaterally (left side) enucleated to section
156 the axons of all motoneurons innervating the extraocular muscles (IIIrd, IVth and VIth
157 nerves). As muscles were also removed, this procedure prevented target reinnervation. In
158 the same surgical session, the left facial nerve was cut and ligated to impede axonal
159 regeneration (for more details on this procedure see Silva-Hucha et al. 2020). After 15
160 days, rats were transcardially perfused with physiological saline followed by 4%
161 paraformaldehyde in PB as explained above for cats. Brainstem vibratome histological
162 50 µm thick sections were obtained. Control data was obtained from the unoperated side.

163 **Immunocytochemical procedures**

164 Free-floating sections were first washed in phosphate-buffered saline, pH 7.4 (PBS) with
165 0.3% TritonX-100 (PBS/TX) and then blocked with normal donkey serum (10% in
166 PBS/TX) for 45 minutes prior to placing the section in primary antibody mixtures. The
167 primary antibodies used were the following: i) goat polyclonal antibody against choline
168 acetyltransferase (ChAT; 1:500; Millipore, Billerica, MA, USA) for the identification of
169 motoneurons; ii) mouse monoclonal antibody against calretinin (1:100; Swant, Burgdorf,
170 Switzerland), a calcium-binding protein that selectively labels the internuclear neurons of
171 the abducens nucleus in cat (de la Cruz et al. 1998); iii) rabbit polyclonal antibody against
172 the rat KCC2 cotransporter (1:500; Millipore) in a region shared by KCC2a and KCC2b
173 isoforms and thus referred as pan KCC2 (pKCC2) or simply as KCC2 ; iv) rabbit
174 polyclonal against the mouse KCC2a N-terminus (aa 20–40) (1:250; kindly provided by
175 Dr. M.S. Airaksinen, University of Helsinki, Finland); v) chicken polyclonal against the
176 mouse KCC2b N-terminus (aa 8–22) (1:750; kindly provided by Dr. M.S. Airaksinen);
177 and vi) mouse monoclonal antibody against activating transcription factor 3 (ATF3;
178 1:200; Novus, CO, USA), which is expressed by axotomized neurons (Tsujino et al.
179 2000). Primary antibodies details, RRID numbers and specificities are shown in Table 2.
180 Briefly, the specificities of antibodies against KCC2 and its isoforms were previously

181 reported using KCC2a-KO or KCC2 null mutation mice (Uvarov et al. 2007; Markkanen
 182 et al. 2014). The ChAT antibody used here efficiently labels brainstem and spinal
 183 motoneurons in cats, rats and mice. The calretinin immunoreactivity shown here was used
 184 as a marker of abducens internuclear interneurons as fully characterized in a previous
 185 report (de la Cruz et al. 1998).

186 **Table 2** Antibodies used in this study

Antigen	Immunogen	Host/ type	Manufacturer	RRID & Specificity	dilution
Pan KCC2	N-terminal His-tag fusion protein of rat KCC2 aa 932-1043	Rabbit/ polyclonal	Millipore Cat #07-432	AB_310611 and AB_11213615	1:500
KCC2a	Mouse KCC2a N-terminus aa 20–40	Rabbit/ polyclonal	Dr M Airaksinen, University of Helsinki, Finland	RRID NA Tested against KCC2a KO ¹	1:250
KCC2b	Mouse KCC2b N-terminus aa 8–22	Chicken/ polyclonal	Dr M Airaksinen, University of Helsinki, Finland	RRID NA Tested by comparison of KCC2 null and KCC2a KO ¹	1:750
ChAT Used for cell type identification	Human placental enzyme	Goat/ polyclonal	Millipore Cat #AB144P	AB_2079751 Identifies Chat expressing motoneurons in Chat-Cre mice	1:500
Calretinin Used for cell type identification	Recombinant human calretinin-22k	Mouse/ monoclonal	Swant Clone 6B3	AB_10000320 Recognizes an epitope within the first 4 EF-hands domains common to both calretinin and calretinin-22k ² Identifies abducens interneurons ³	1:100
ATF3 Used for injured motoneuron identification	Recombinant protein corresponding to aa 1-103 in human ATF3	Mouse/ monoclonal	Novus Clone 1685 NBP2-34489	AB_2786997 Recognizes the epitope: ASAIVPCLSPPGSL (Manufacturer's information) Not present in uninjured motoneurons	1:200

18718
 7

188 Secondary antibodies were all obtained from Jackson ImmunoResearch (West Baltimore
 189 Pike, West Grove, PA, USA), used at a dilution 1:100 in PBS/TX and were the following:
 190 i) donkey anti-goat IgG coupled to FITC (for ChAT detection); ii) donkey anti-mouse
 191 IgG coupled to Cy5 (to label calretinin); iii) donkey anti-rabbit IgG coupled to Cy3 (for
 192 KCC2 detection); iv) donkey anti-rabbit IgG coupled to Cy5 (to reveal KCC2a); v)
 193 donkey anti-chicken IgY coupled to FITC (for KCC2b visualization); and donkey anti-

194 mouse IgG coupled to Cy5 (for ATF3 detection). Finally, sections were rinsed in PBS,
195 mounted on glass slides and coverslipped with Vectashield mounting medium (Vector
196 Laboratories, Burlingame, CA, USA).

197 **Microscopy and imaging**

198 A confocal microscope (Olympus FLUOVIEW FV1000) was used to capture image z-
199 stacks of areas and cells of interest at X10 and X60 for panoramic and high-magnification
200 images, respectively. Acquisition parameters were adjusted to use the maximum dynamic
201 range of the images and kept constant to allow comparisons among neurons and animals.
202 Confocal images were analyzed using Image J (NIH, Bethesda, MD, USA). To quantify
203 the intensity of KCC2 immunofluorescence on the motoneuron surface, we selected focal
204 planes at mid-nuclear level in which membrane KCC2 immunoreactivity was orthogonal
205 to the plane of view. In each section, background measurements were taken from a $9\ \mu\text{m}^2$
206 square region of the neuropil in the same optical plane, next to the motoneurons and
207 lacking any somatic or dendritic labeling. Average KCC2 immunofluorescence was
208 measured on line profiles along the surface of the motoneurons and corrected for
209 background level by calculating the percentage higher than background [$100 \times$
210 (membrane intensity average – background intensity average)/average background
211 intensity], as previously described (Akhter et al. 2019). Because we used non-serial
212 sections for all the analyses and the mid-cell optical section is restricted to a few confocal
213 planes within one histological section it was impossible that the same individual
214 motoneuron was resampled during KCC2 quantitation. In other words, our samples are
215 independent motoneuron cross sections each belonging to a different motoneuron.

216 **Physiological analysis**

217 The discharge characteristics of cat abducens motoneurons have been previously
218 described (Delgado-García et al. 1986a; Davis-López de Carrizosa et al. 2011). Abducens

219 motoneurons display a tonic-phasic firing pattern that is proportional to eye position and
220 velocity, respectively. The slope of the regression line between tonic firing rate and eye
221 position during gaze holding corresponds to the neuronal eye position sensitivity (k , in
222 spikes/s/degree). During spontaneous rapid eye movements or saccades, the slope of the
223 regression line between firing rate and eye velocity is the neuronal eye velocity sensitivity
224 (r , in spikes/s/degree/s). In the present study, we calculated these two parameters
225 separately depending on the direction of eye movement with the aim of differentiating
226 the motoneuronal signals encoded during excitatory *versus* inhibitory premotor drive.
227 Thus, firing rates during eye fixations after saccades occurring in the direction of
228 motoneuronal activation were correlated with eye position yielding the k -on parameter.
229 On the other hand, the rate-position correlation during eye fixations following saccades
230 in the direction of inactivation produced the k -off parameter. Similarly, r -on and r -off
231 parameters were calculated from the rate-velocity correlation separating those saccades
232 occurring in the direction of motoneuronal activation from those in the direction of
233 inactivation (Delgado-García et al. 1986a,b).

234 **Statistics**

235 Comparisons between two groups were performed using either the Mann-Whitney rank
236 sum test or the Student t-test. For comparisons between more than two groups, we used
237 the Kruskal-Wallis one-way ANOVA test followed by Dunn's method for *post hoc*
238 pairwise multiple comparisons, or either the one-way or the two-way ANOVA test
239 followed by the *post hoc* Holm-Sidak method, in all cases at an overall significance level
240 of 0.05. Statistics was carried out using SigmaPlot 11 (Systat Software, Inc., Chicago, IL,
241 USA). When a significant difference was detected, effect sizes were measured by Cohen's
242 d , that calculates differences between samples as multiples (or fractions) of the average
243 standard deviation of the samples.

244 In all comparisons we pooled together motoneurons recorded in similar conditions from
245 all animals. “n” therefore represents the number of motoneurons in all statistical
246 comparisons. There are several justifications for this experimental design: 1) It reduces
247 the number of cats used in these studies following ethical guidelines for minimizing the
248 use of animals in research; 2) A recent thorough statistical analysis of motoneurons
249 differences in ALS vs wildtype animals suggested that n = motoneurons provides a
250 rigorous comparison, sometimes better than grouping data per animal averages, and also
251 better describes the distribution of data points and variability in the population than
252 animal averages which obscure possible differences among different motoneurons
253 (Dukkipati et al., 2017); 3) n = motoneurons parallels common experimental designs and
254 data analyses in electrophysiological experiments to which the anatomical data was
255 directly compared; 4) The larger samples obtained by treating individual motoneurons as
256 data points allow us to increase rigor when estimating effects sizes and their significance
257 using estimating statistics by bootstrapping subsample data sets (Ho et al., 2019). We
258 were careful to analyze similar numbers of motoneurons in each animal and to confirm
259 lack of interanimal variability before pooling together all the data. In text, sample
260 structures are always described as average number of motoneurons \pm S.D. per animal.

261 We used bootstrapping according to the method of Ho et al., (2019) to estimate effect
262 sizes and the significance of differences between control and experimental motoneurons.
263 5,000 bootstrap samples were taken to calculate average differences and their 95%
264 confidence intervals bias-corrected and accelerated. In this comparison p values report
265 the likelihood of observing the effect size if the null hypothesis of zero difference is true.
266 If $p < 0.05$ we interpret that the difference between means is significantly different from
267 0. In all cases considered significant the distribution of subsample differences display
268 95% CI limits that do not cross 0.

269 Quantitative data represented with histogram plots indicates mean \pm standard error of the
270 mean (SEM) whereas whisker box plots show the median, 25th and 75th quartiles with
271 90th and 10th percentile error bars. Estimated differences are represented as a Gaussian
272 with the 95% confidence limit interval superimposed. All individual data points are
273 graphed adjacent to summary graphs in swarm plots.

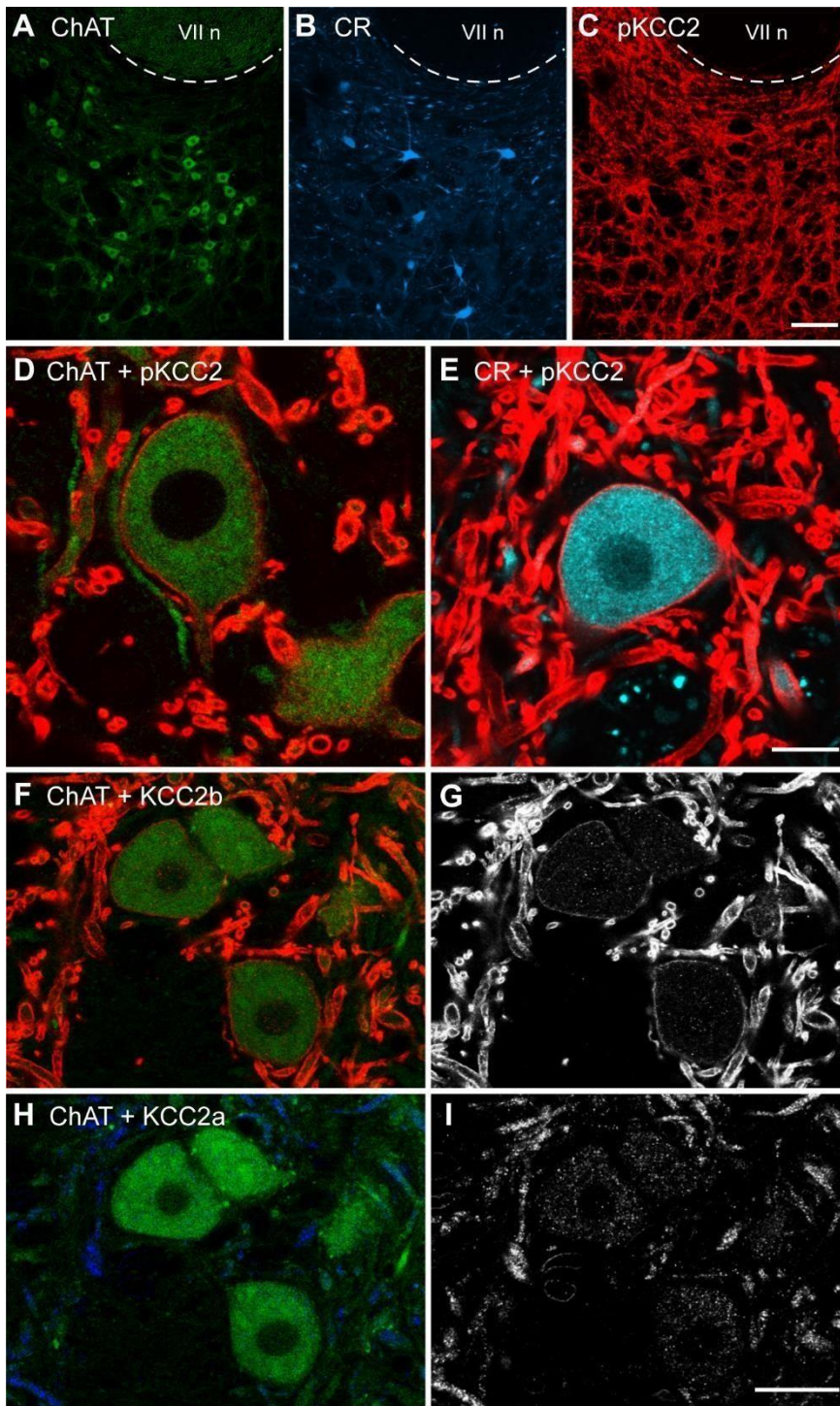
27427
4

275 **Results**

276 **KCC2 expression in abducens neurons**

277 The abducens nucleus contains two types of neurons, motoneurons which innervate the
278 ipsilateral lateral rectus muscle, and internuclear neurons whose axons project to
279 contralateral medial rectus motoneurons in the oculomotor nucleus. In brainstem sections,
280 the abducens nucleus was identified by locating motoneurons and internuclear neurons
281 with ChAT (Fig. 1A, green-FITC) and calretinin (CR) immunolabeling, respectively (Fig.
282 1B, cyan-Cy5) (de la Cruz et al. 1998). The abducens nucleus showed also high pan-
283 (p)KCC2 immunoreactivity (detecting all KCC2 isoforms) at low magnification (Fig. 1C,
284 red-Cy3). At high magnification, the strongest pKCC2 immunoreactivity was found on
285 the many small dendrites that traversed the abducens nucleus, while pKCC2

286 immunoreactivity on the surface of cell bodies was weaker.



287

288 **Figure 1. Presence of KCC2 and KCC2 isoforms in the cat abducens nucleus.**

289 Moreover, pKCC2 immunoreactivity on the cell bodies of ChAT-immunoreactive
290 motoneurons (Fig. 1D) was consistently less intense than over the cell bodies of CR-
291 immunoreactive internuclear neurons (Fig. 1E). To best quantify this difference, we set

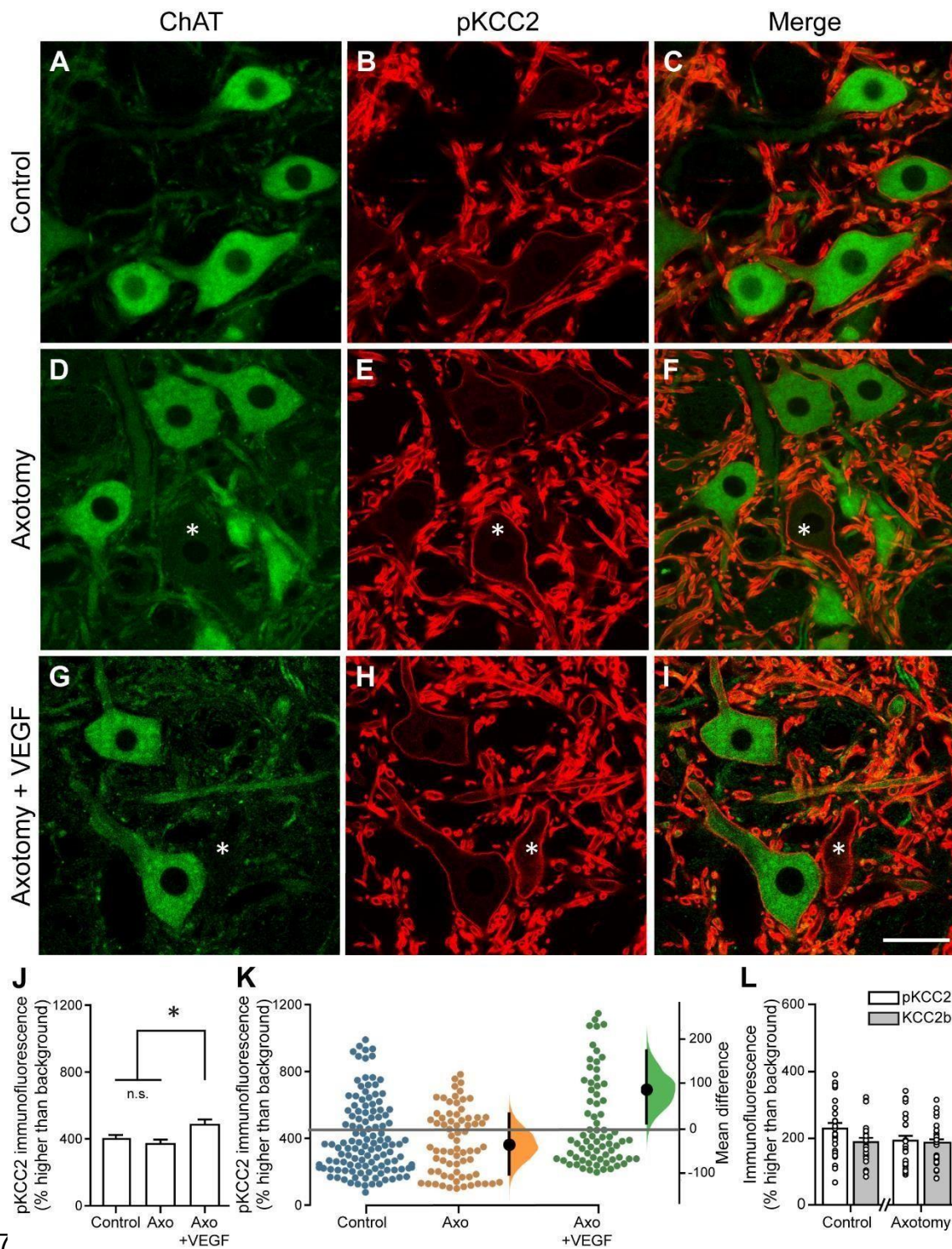
292 image acquisition parameters to maximize dynamic resolution of cell body
293 immunofluorescence, although this frequently saturated dendritic labeling. A Mann-
294 Whitney rank sum test comparing pKCC2 immunofluorescence (% higher than
295 background) on the cell bodies of motoneurons ($n = 122$) and internuclear neurons ($n =$
296 37) demonstrated significantly higher levels of KCC2 in internuclear neurons ($p = 0.005$,
297 $U = 1571$, Cohen's $d = 0.455$).

298 The mammalian *kcc2* gene generates two isoforms, KCC2a and KCC2b (Uvarov
299 et al. 2007). We used isoform specific antibodies to analyze their specific cellular
300 localization with triple immunofluorescence against ChAT, KCC2a and KCC2b in both
301 the abducens nucleus and the spinal cord motoneurons. Immunolabeling with KCC2b was
302 similar in appearance to that with pKCC2, both strongly expressed on the surface of
303 dendrites and clearly delineating the somatic plasma membrane of motoneurons (Fig. 1F-
304 G). In contrast, KCC2a immunolabeling yielded mostly intracellular labeling in soma and
305 dendrites of ChAT-positive motoneurons (Fig. 1H-I). Similar results were obtained in the
306 spinal cord.

30730
7

308 Axotomy does not modify KCC2 levels in cat abducens motoneurons and VEGF
309 induces an upregulation

310 We expected that, in accordance with other cranial and spinal motoneurons, abducens
311 motoneurons would downregulate KCC2 expression following axotomy and we
312 hypothesized KCC2 downregulation could be prevented with VEGF, because this
313 neurotrophic factor fully recovers the discharge alterations induced by axotomy in
314 abducens motoneurons (Calvo et al. 2018, 2020). Double immunofluorescence was
315 carried out for ChAT and pKCC2 in control and axotomized motoneurons treated or not
316 with VEGF (Fig. 2A-I). For these analyses we pooled all motoneurons sampled from 6



317317

318 **Figure 2. Changes in KCC2 levels induced by axotomy and VEGF administration in**
 319 **cat abducens motoneurons.**

320 control abducens ($n = 122$ motoneurons; 20.3 ± 3.9 average per animal \pm S.D.), 3

321 axotomized ($n = 71$ motoneurons; 23.7 ± 3.8) and 3 axotomized treated with VEGF ($n =$

322 72 motoneurons; 24.0 ± 2.9). After the interval of 3 weeks post-lesion surprisingly

323 pKCC2 immunolabeling surrounding injured abducens motoneurons was unchanged
324 compared to control (Fig. 2A-C vs. D-F). In contrast, motoneurons treated with VEGF
325 showed higher levels (Fig. 2G-I). Abducens internuclear neurons (ChAT-negative,
326 marked by an asterisk in Fig. 2D-I) displayed their normal high levels of pKCC2 in all
327 conditions. A one-way ANOVA test revealed the existence of significant differences on
328 pKCC2 immunofluorescence among axotomized motoneurons treated with VEGF,
329 untreated axotomized and control motoneurons (Fig. 2J; $F_{(2, 262)} = 4.671$, $p = 0.01$, $d =$
330 0.486). Pairwise multiple comparisons (Holm-Sidak method) demonstrated that there was
331 no difference between control and axotomy ($p = 0.394$), whereas axotomized + VEGF-
332 treated motoneurons showed significantly higher pKCC2 immunofluorescence than both
333 control ($p = 0.017$) and axotomy ($p = 0.004$). In summary, axotomy did not downregulate
334 KCC2 in abducens motoneurons but VEGF increased significantly the level of membrane
335 KCC2 detected with immunofluorescence.

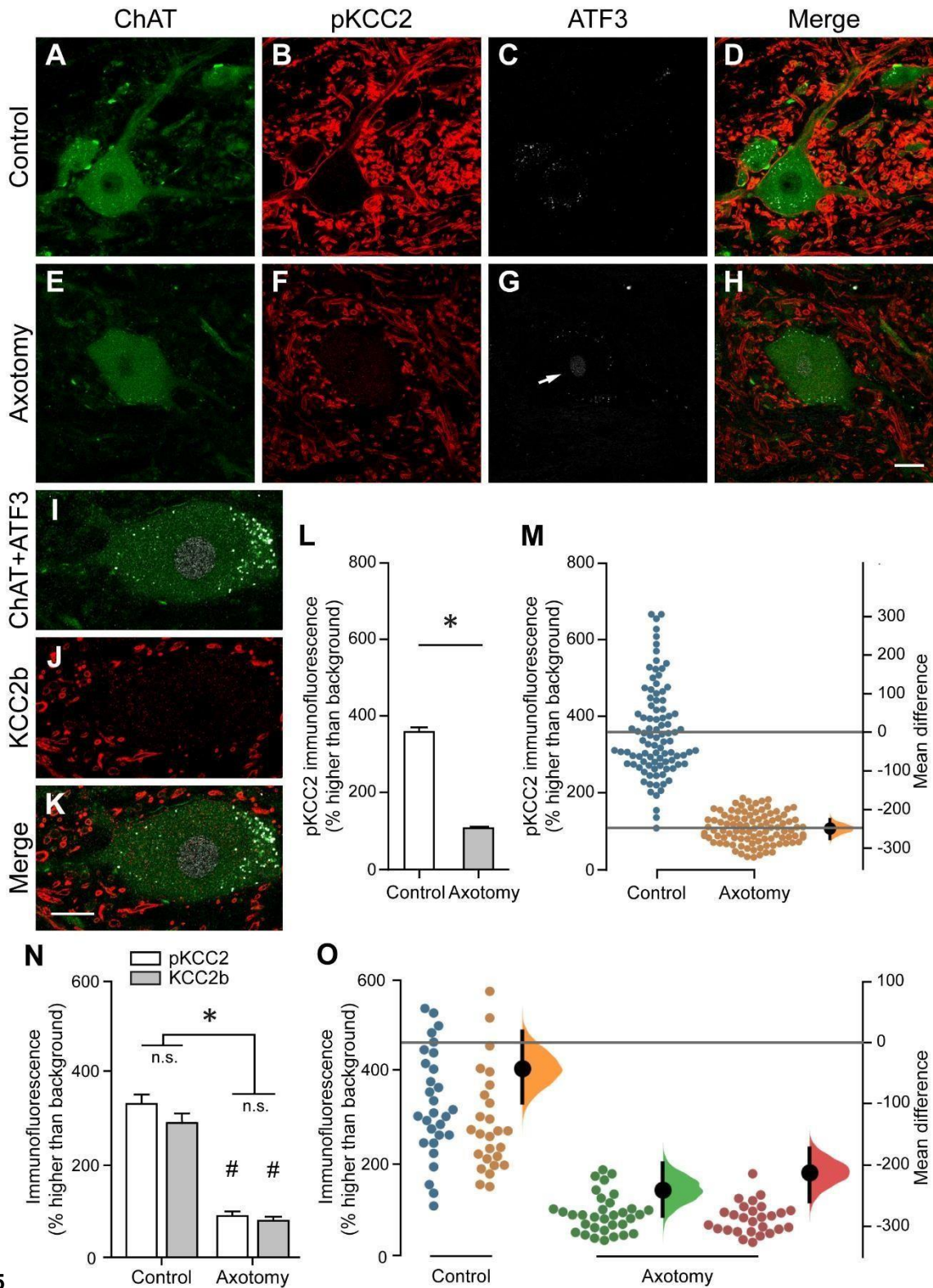
336 To further define the increase in pKCC2 we used estimation statistics (Fig. 2K). For this
337 purpose, 5,000 bootstrap data set were obtained to perform aleatory comparisons between
338 subsample pairs and estimate an average difference and 95% confidence intervals (CI)
339 for the size of possible differences and their significance using a two-sided permutation
340 t-test. Comparisons between control ($n = 122$) and axotomized motoneurons ($n = 71$)
341 indicated that the 95% CI of average differences between axotomized motoneurons and
342 controls ranged from a 22% decrease to an 8% increase with $p = 0.366$ (2-sided
343 permutation t-test) suggesting lack of significance. However, when comparing control
344 motoneurons to VEGF-treated animals the 95% CI for their differences ranged between
345 4% to 40% increases with $p = 0.026$ (2-sided permutation t-test) and the average estimated
346 difference suggested a 21% increase in KCC2 immunofluorescence pixel density
347 surrounding the cell body compared to control and 22% increase when compared to non-

348 VEGF treated axotomized motoneurons. This effect correlated with a functional
349 enhancement of inhibition, as shown below.

350 **Preservation of KCC2 in axotomized cat abducens motoneurons is not a species-**
351 **specific phenomenon**

352 The lack of KCC2 change in axotomized cat abducens motoneurons contrasted markedly
353 with the strong downregulation known to occur in spinal and other brainstem
354 motoneurons following their axotomy in rodents (Nabekura et al. 2002; Tatetsu et al.
355 2012; Kim et al. 2018; Akhter et al. 2019). To discard the possibility that cat motoneurons
356 in general lack KCC2 regulation after axotomy, we analyzed axotomized spinal
357 motoneurons in the cat. For this purpose, the tibial nerve was cut in three cats and a
358 ligature made in the proximal stump of the nerve to prevent regeneration. Twenty-one
359 days later, tissue from these animals was processed for triple immunofluorescence ChAT,
360 pKCC2 and ATF3. Control spinal motoneurons were identified in the contralateral side
361 by ChAT (Fig. 3A), they displayed pKCC2 on the somatic membrane (Fig. 3B), and
362 lacked ATF3 nuclear labeling (Fig. 3C) ($n = 96$ control motoneurons; 32.0 ± 2.9 per
363 animal). ChAT and ATF3 were used to positively identify axotomized spinal
364 motoneurons (Fig. 3E-G) ($n = 101$ axotomized motoneurons; 33.7 ± 1.7 per animal). They
365 lacked pKCC2 on their membrane (Fig. 3F). Figures 3D, H illustrate the merge of the
366 triple immunofluorescence in a control and an axotomized motoneuron, respectively. In
367 contrast to cat abducens motoneurons, axotomized ATF3-positive spinal cat motoneurons
368 significantly downregulated pKCC2 (Fig. 3L; t-test, $p \leq 0.001$, $t_{(195)} = 20.142$). Estimation
369 of effect size differences suggested this was close to 3 standard deviations ($d = 2.871$)
370 with a 95% CI ranging from a 63% to 77% decreases in pKCC2 pixel density, averaging
371 a 70% decrease that was highly significant ($p < 0.0001$, 2-sided permutation test) (Fig.
372 2M). These findings suggest that spinal motoneurons in the cat downregulate KCC2

373 normally after axotomy and that the absence of change in abducens motoneurons is not a
 374 general response of cat motoneurons, but specific to the abducens nucleus.



375

376 **Figure 3. KCC2 changes induced by axotomy in cat spinal motoneurons.**

377 KCC2b is the preferential isoform present and regulated on the motoneuron cell
378 body

379 KCC2b and pKCC2 showed similar distributions on the somatic membrane of abducens
380 and spinal motoneurons. Thus, we compared whether both are co-regulated after axotomy
381 in spinal and abducens motoneurons. Comparisons between both immunostainings were
382 done in control and axotomized motoneurons obtained from one cat in the abducens
383 nucleus (Fig. 1F-G and 2N) and one cat in the spinal cord (Fig. 3I-K and N). Two-way
384 ANOVA for KCC2 immunoreactivity (pKCC2 or KCC2b), experimental condition
385 (control or axotomized) and any possible interaction (Fig. 2K) found no significant
386 differences in abducens motoneurons (pKCC2 vs KCC2b, $p = 0.089$, $F_{(1,108)} = 2.937$;
387 control vs. axotomized, $p = 0.166$, $F_{(1,108)} = 1.946$; interaction, $p = 0.207$, $F_{(1,108)} = 1.611$;
388 $n = 27$ and 24 control and $n = 29$ and 32 axotomized motoneurons analyzed for pKCC2
389 and KCC2b respectively in each experimental situation). In the spinal cord a similar two-
390 way ANOVA (Fig. 3M) detected a significant reduction in control vs. axotomized
391 motoneurons ($p < 0.001$, $F_{(1,111)} = 207.044$; $n = 29$ and 26 control and $n = 33$ and 27
392 axotomized motoneurons for respectively pKCC2 and KCC2b; Cohen's $d = -2.8$ for
393 pKCC2 and -2.6 for KCC2b), but there was no difference between pKCC2 and KCC2b
394 (they changed in parallel) ($p = 0.099$, $F_{(1,111)} = 2.763$) or the interaction between axotomy
395 and type of immunoreactivity ($p = 0.334$, $F_{(1,111)} = 0.942$,). *Post-hoc* Holm-Sidak methods
396 revealed significant difference between control and injured motoneuron for pKCC2 and
397 KCC2b ($p < 0.001$ for both). However no significant differences in somatic membrane
398 immunofluorescence were found between pKCC2 and KCC2b in control ($p = 0.071$) or
399 axotomy ($p = 0.619$).

400 To further support similar regulation of pKCC2 and KCC2b in spinal motoneurons we
401 compared the effect of axotomy on the decrease of each immunofluorescence in a single

402 animal in which pKCC2 and KCC2b were compared in parallel. We found that the 95%
403 CI of the difference to control suggested a decrease in pKCC2 ranging from 60% to 85%
404 with an average of 72% decrease with respect to control value and this was highly
405 significant ($p < 0.0001$, 2-sided permutation test). KCC2b depletions paralleled the
406 decrease in pKCC2 with a 95% CI decrease ranging from 59% to 88%, averaging a highly
407 significant 72% decrease ($p < 0.0001$, 2-sided permutation t-test) (Fig. 3O). KCC2b is
408 therefore the isoform principally expressed and regulated on the somatic plasma
409 membrane of abducens and spinal motoneurons and pKCC2 and KCC2b
410 immunoreactivities are interchangeable in this model.

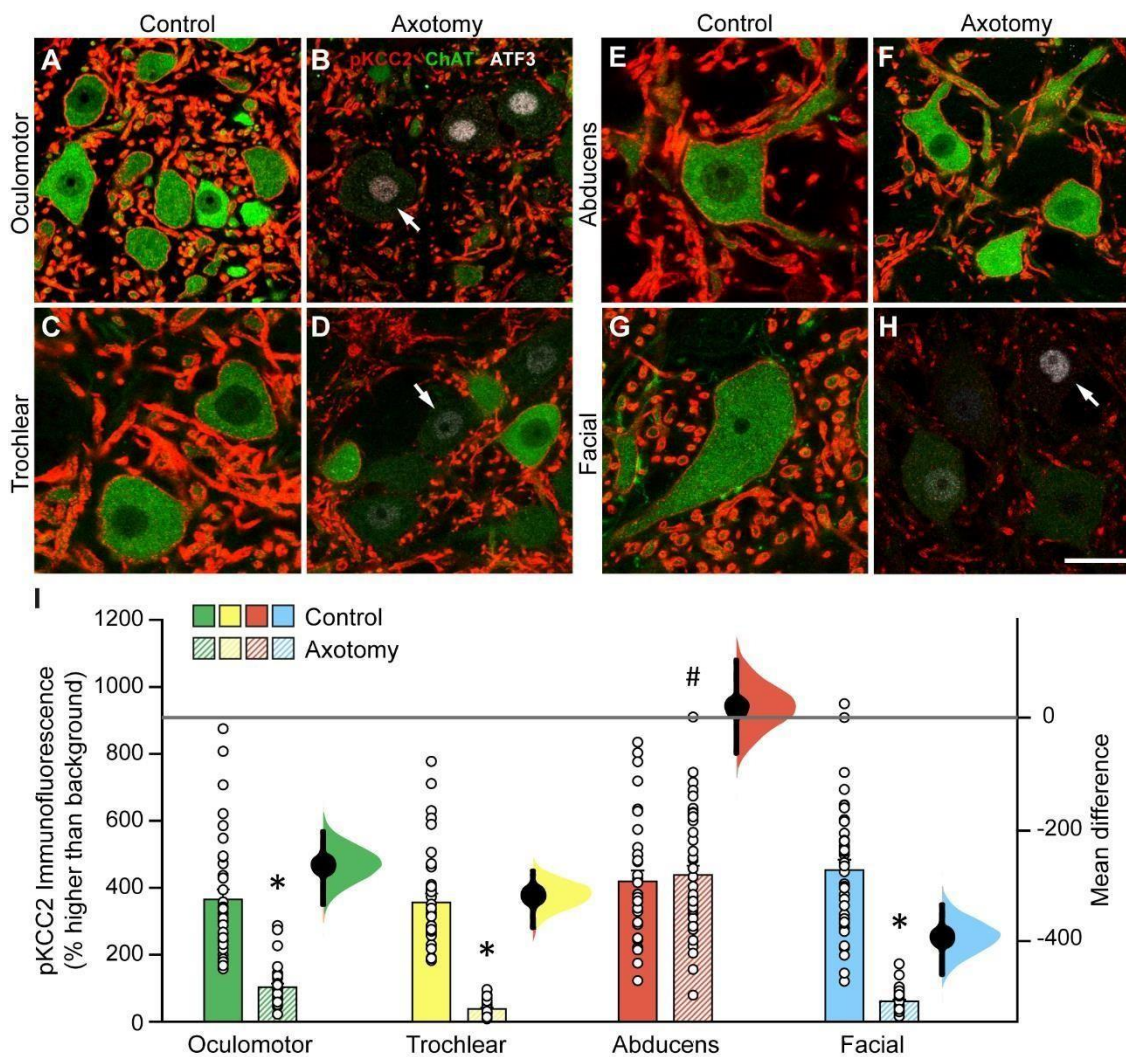
41141
1

412 Abducens motoneurons are unique across species in their preservation of KCC2
413 among brainstem motoneurons

414 Next, we analyzed whether the absence of change in KCC2 after axotomy in abducens
415 motoneurons was unique to the cat by comparing KCC2 regulation after axotomy in the
416 rat abducens nucleus. We compared KCC2 regulation after axotomy in the motoneurons
417 of the three oculomotor nuclei (abducens, trochlear and oculomotor) as well as in other
418 cranial motoneurons (facial nucleus). For this purpose, three adult rats were enucleated
419 unilaterally (left side), a procedure that axotomizes all extraocular motoneurons and leave
420 them target deprived. In the same surgical session, the left facial nerve was also sectioned
421 as a reference, since it is well-established that axotomized facial motoneurons in the rat
422 downregulate KCC2 expression (Toyoda et al. 2003). KCC2 levels were evaluated 15
423 days postlesion in the four brainstem nuclei by means of triple immunofluorescence
424 against ChAT, pKCC2, and ATF3 and compared to control motoneurons in the
425 contralateral side. pKCC2 immunofluorescence was markedly decreased in axotomized
426 oculomotor (Fig. 4A-B; the white arrow points to nuclear ATF3 staining, as a marker of

427 neuronal injury), trochlear (Fig. 4C-D) and facial (Fig. 4G-H) motoneurons. In contrast -
428 as happened in the cat- rat abducens motoneurons displayed similar pKCC2 in axotomy
429 and control. In addition, and in parallel with the cat, ATF3 did not label rat axotomized
430 abducens motoneurons (Fig. 4E-F). Quantification of pKCC2 immunofluorescence in all
431 nuclei was compared using a two-way ANOVA test (two factors: nucleus and treatment)
432 followed by Holm-Sidak method for pairwise comparisons (Fig. 4I). Axotomized
433 oculomotor, trochlear and facial motoneurons had significantly lower KCC2
434 immunofluorescence than their respective controls (Fig. 4I, asterisks; $p < 0.001$ for the
435 three motoneuronal types). No significant differences were found between axotomized
436 and control abducens motoneurons ($p = 0.564$). The three oculomotor nuclei exhibited a
437 similar value of pKCC2 immunofluorescence in the control situation (abducens *vs.*
438 oculomotor $p = 0.128$; abducens *vs.* trochlear $p = 0.081$; oculomotor *vs.* trochlear $p =$
439 0.827), while the facial nuclei had slightly higher pKCC2 immunoreactivity compared to
440 oculomotor ($p = 0.021$) and trochlear ($p = 0.011$), but not when compared against
441 abducens ($p = 0.445$). Axotomized motoneurons drastically downregulated KCC2
442 immunofluorescence to similar low levels in oculomotor, trochlear and facial, but not in
443 the abducens. As a result, axotomized abducens motoneurons showed a significantly
444 higher value of pKCC2 labeling than the other three motoneuronal types after axotomy
445 (Fig. 4I, hashtag; $p < 0.001$ for all cases; $n = 35, 36, 33$ and 39 motoneurons for control
446 and $n = 33, 35, 44$ and 42 for axotomized motoneurons of the oculomotor, trochlear,
447 abducens and facial nuclei, respectively, Cohens' $d = -1.9$ for oculomotor, -3.0 fr trochlear
448 and -2.9 for facial). Estimated differences after creating bootstrapped datasets ranged
449 from 57% to 100% depletions from control with average reductions of 72%, 89% and
450 87% membrane pKCC2 immunoreactivity, respectively for oculomotor, trochlear and
451 facial motoneurons, and in all cases this being highly significant ($p < 0.001$, 2-side
452 permutation t-test). This was not the case for abducens axotomized motoneurons which

453 showed no significant effect in pKCC2 immunoreactivity compared to controls ($p =$
 454 0.655; 2-sided permutation t-test; average estimated difference <5% from control, with a
 455 broad range in different bootstrapped data sets ranging in 95% CI from 15% depletion to
 456 a 24% increase).



457457

458 **Figure 4. KCC2 immunoreactivity in brainstem oculomotor, trochlear, abducens**
 459 **and facial motoneurons, in control and after axotomy, in the rat.**

460 In conclusion, preservation of KCC2 in axotomized abducens motoneurons was
 461 similar in cats and rats. Since nerve injury in our rat surgical model occurs simultaneously
 462 and by the same procedure (eye enucleation) in all three groups of extraocular
 463 motoneurons, we can exclude the possibility of differential levels of injury, and conclude

464 that the response to axotomy of abducens motoneurons is unique to them across species
465 and not a general feature of extraocular motoneuronal nuclei.

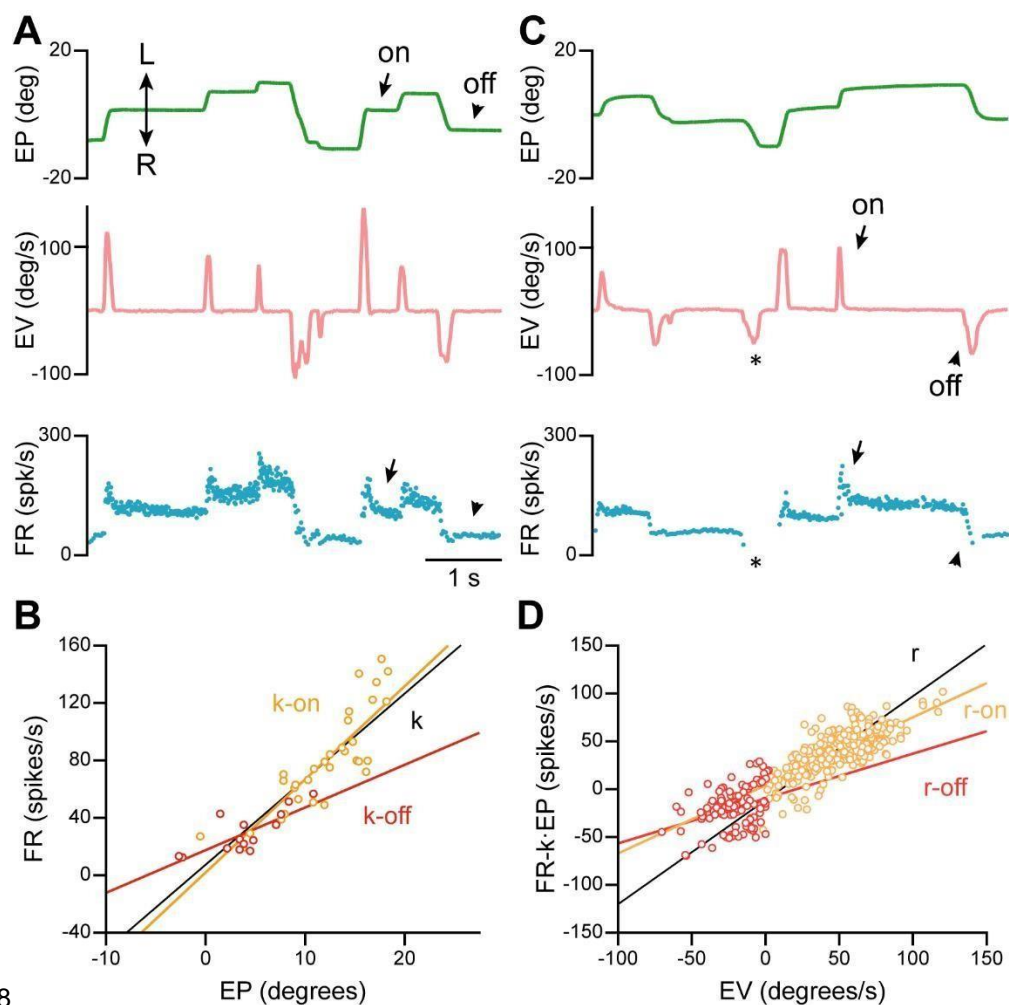
46646
6

467 Discharge signals derived from inhibitory synapses increase by VEGF in axotomized
468 abducens motoneurons

469 Control abducens motoneurons have a tonic-phasic firing pattern that correlates with eye
470 position and velocity (Delgado-García et al. 1986a; Davis-López de Carrizosa et al.
471 2011). These motoneurons discharge monotonically at higher frequencies for gaze
472 fixations set at more eccentric eye positions in the direction of activation (on-direction)
473 and decrease their firing rate for those fixations in the off-direction (Fig. 5A). Therefore,
474 there is a correlation between firing rate and eye position in control motoneurons (Fig.
475 5B). The slope of this regression line is named k (in spikes/s/degree; black line in Fig.
476 5B). The tonic component of the discharge can be analyzed differentiating between those
477 fixations occurring after an on-directed saccade (arrows in Fig. 5A) *versus* those
478 occurring after an off-directed saccade (arrowheads in Fig. 5A). This led to two distinct
479 rate-position correlations, after separating those fixations following on-saccades from
480 those attained after off-saccades. Therefore, two regression lines were obtained whose
481 slopes were k -on (orange line and dots in Fig. 5B) and k -off (red line and dots in Fig 5b),
482 being k -on related to modulation of excitatory inputs (increases in firing) and k -off related
483 to modulation of inhibitory inputs (decreases in firing).

484 Control abducens motoneurons also exhibit a phasic component, displayed in the
485 form of a high-frequency burst of spikes for those saccades in the on-direction (arrows in
486 Fig. 5C) and an abrupt decay in firing rate or a pause for off-directed saccades
487 (arrowheads in Fig. 5C). Those off-saccades resulting from a cease in motoneuronal
488 discharge (asterisks in Fig. 5C) were not considered for the analysis. The correlation

489 between firing rate (previous subtraction of the eye position component) and eye velocity
 490 during saccades fits to a regression line whose slope is the neuronal eye velocity
 491 sensitivity (r , in spikes/s/degree/s; black line in Fig. 5D). When the rate-velocity
 492 correlation was performed separating on- *versus* off-saccades, then the parameters r -on
 493 (orange line and dots in Fig. 5D) and r -off (red line and dots in Fig. 5D) were obtained
 494 (for more details see Delgado-García et al. 1986a,b). k -on and r -on represent the
 495 excitatory drive in abducens motoneurons arising from specific excitatory inputs, whereas
 496 k -off and r -off are the result of the inhibitory drive originating from inhibitory inputs to
 497 the abducens nucleus (Escudero and Delgado-García 1988; Escudero et al. 1992).



498

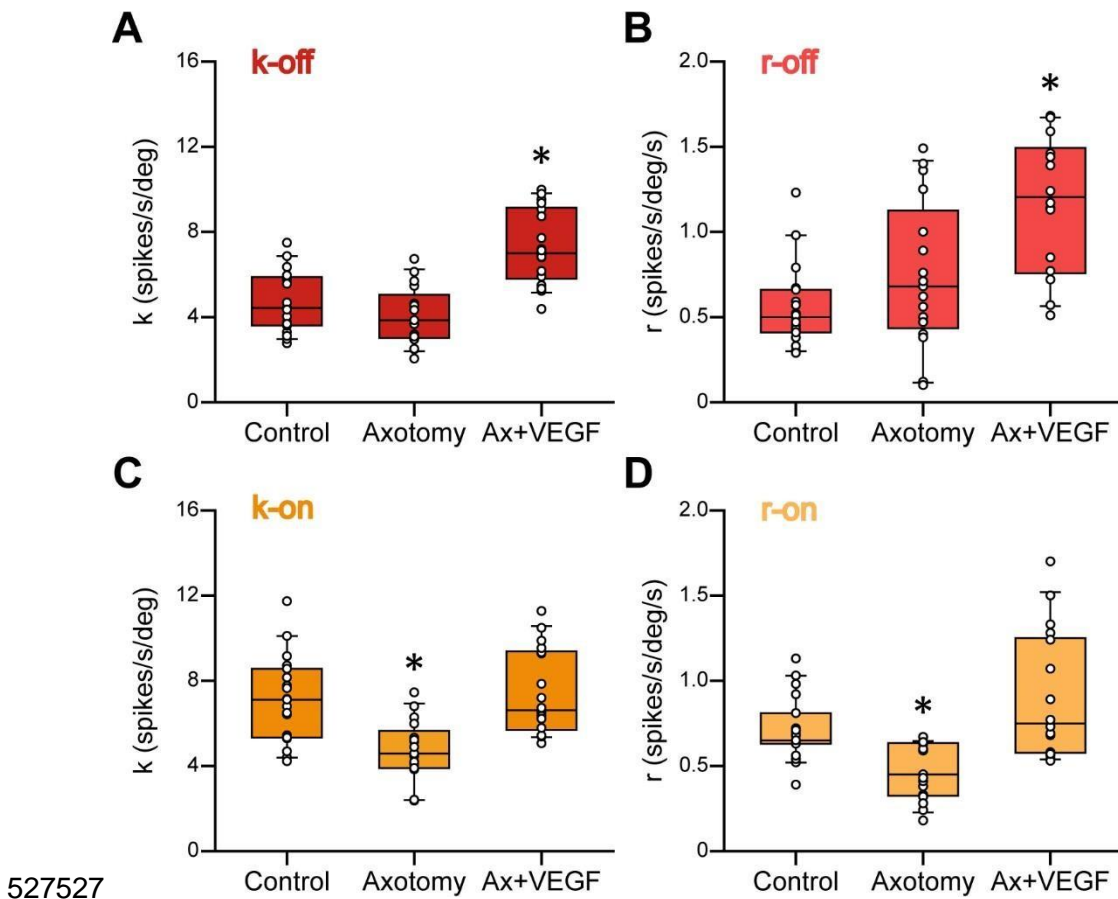
499 **Figure 5 Procedure to calculate k -on, k -off, r -on and r -off in the discharge activity**
 500 **of abducens motoneurons.**

501 We compared the excitatory signals, k-on and r-on, and the inhibitory signals, k-off and
502 r-off, in abducens motoneurons under the different situations (control, axotomy, axotomy
503 + VEGF) to determine whether there was a correlation between KCC2 level and
504 inhibitory synaptic drive. Neurophysiological recordings were re-analyzed from our
505 previous work (Calvo et al. 2018) (control, $n = 21$; axotomy, $n = 17$; axotomy + VEGF,
506 $n = 18$). Significant differences were detected among the three groups for k-off (Kruskal-
507 Wallis one-way ANOVA test, $p \leq 0.001$, $H = 23.625$, $d = 1.66$) and r-off (Kruskal-Wallis
508 one-way ANOVA test, $p \leq 0.001$, $H = 19.441$, $d = 1.401$). Dunn's pairwise multiple
509 comparisons showed higher k-off and r-off in abducens axotomized motoneurons treated
510 with VEGF compared with untreated control and axotomized motoneurons (asterisks in
511 Fig. 6A-B; $p < 0.05$ for k-off as well as r-off), whereas there was no significant difference
512 in k-off and r-off between control and axotomized abducens motoneurons ($p > 0.05$).

513 On the other hand, axotomized abducens motoneurons treated with VEGF had
514 similar k-on and r-on values compared to control ($p > 0.05$ for both; $Q = 0.668$ for k-on
515 and $Q = 1.514$ for r-on, Dunn's pair-wise comparisons), whereas axotomized
516 motoneurons presented significantly lower k-on ($p < 0.05$, $Q = 3.379$) and r-on than
517 control ($p < 0.05$, $Q = 2.876$) and or axotomized VEGF-treated motoneurons ($p < 0.05$
518 for both, $Q = 3.894$ for k-on and $Q = 4.212$ for r-on) (Fig. 6 C-D). For comparisons
519 between the three groups, Kruskal-Wallis one-way ANOVA test was used ($p \leq 0.001$, H
520 $= 17.540$, $d = 1.288$, for k-on; $p \leq 0.001$, $H = 18.326$, $d = 1.334$, for r-on), followed by
521 Dunn's method for all pairwise multiple comparisons.

522 Therefore, inhibition increase (larger k-off and r-off) in axotomized motoneurons
523 treated with VEGF correlated with the findings of higher levels of KCC2
524 immunofluorescence in axotomized + VEGF-treated abducens motoneurons, which

525 likely led to larger Cl^- extrusion and a more hyperpolarized E^- , which strengthens
526 inhibitory synaptic transmission.



527527
528 **Figure 6. Quantitative analysis of neuronal sensitivities to eye position and velocity**
529 **depending on the on- or off-direction of the fixation or saccade.**

530530

531 **Discussion**

532 The present results show that axotomy did not modify KCC2 in abducens motoneurons
533 of cats and rats, in contrast to the downregulation in other brainstem and spinal
534 motoneurons after axotomy in both species. This suggests that abducens motoneurons are
535 unique in the lack of KCC2 regulation after axotomy. Our findings also indicated that the
536 expression and changes in KCC2 at the soma surface of motoneurons were due mainly to

537 the KCC2b isoform. Finally, administration of VEGF to axotomized abducens
538 motoneurons significantly upregulated the levels of KCC2 above control and axotomy,
539 and this correlated with an increase in off-related discharges of abducens motoneurons
540 recorded in alert cats. Previous studies highlighted BDNF as an important regulator of
541 KCC2 expression during development and after injuries or neuropathology in adults (Lee-
542 Hotta et al. 2019). Our results suggest, however, that in motoneurons, VEGF regulates
543 KCC2 expression. Since VEGF is produced by muscle, and KCC2 expression in
544 motoneurons depend on muscle innervation (Akhter et al. 2019), it is possible that VEGF
545 could act as a target-derived neurotrophic factor (Calvo et al. 2018, 2020) modulating
546 KCC2 expression in motoneurons.

54754
7

548 Differential regulation of KCC2 in abducens and spinal motoneurons after axotomy

549 The most striking result was that abducens motoneurons did not downregulate KCC2 after
550 axotomy despite using a method extensively validated for chronic axotomy of abducens
551 motoneurons in the cat (David López de Carrizosa et al. 2008, 2009, 2010; Calvo et al.
552 2018, 2020). The absence of change was not generalizable to all extraocular motoneurons,
553 since oculomotor and trochlear motoneurons downregulated KCC2 after axotomy, similar
554 to other spinal and brainstem motoneurons studied to date in rodents (Nabekura et al.
555 2002; Toyoda et al. 2003; Tatetsu et al. 2012; Kim et al. 2018; Akhter et al. 2019). A cat-
556 specific response does not explain KCC2 preservation either, since axotomized spinal
557 motoneurons in the cat showed normal KCC2 downregulation after axotomy, and rat
558 abducens motoneurons did not downregulate KCC2, similar to the cat. In parallel, ATF3
559 was not expressed by axotomized abducens motoneurons. ATF3 upregulation is a
560 consistent phenomenon in all previously studied motoneurons and sensory neurons after
561 axotomy (Tsuji no et al. 2000; Holland et al. 2019) and is part of signaling cascades

562 leading to coordinated stress and/or regeneration responses in neurons (Patodia and
563 Raivich 2012). However, although ATF3 enhances regeneration, alone does not entirely
564 recapitulate the whole regenerative program (Seijffers et al. 2007), and its deletion does
565 not fully prevent axon regeneration (Gey et al. 2016; Holland et al. 2019). This suggests
566 the possibility of a multiplexed response to injury that might not be identical for every
567 motoneuron. It is possible that abducens motoneurons are at one extreme of a diversity of
568 motoneuronal responses to injury and regeneration, being in this case ATF3-independent
569 and preserving KCC2 expression. Whether there is a causal link between ATF3
570 upregulation and KCC2 downregulation needs to be further studied. Nonetheless, many
571 other properties of axotomized motoneurons are present in abducens motoneurons; these
572 include changes in physiological properties, synaptic plasticity and neighboring glial
573 reactions (Delgado-García et al. 1988; Davis-López de Carrizosa et al. 2009, 2010). The
574 possible implications for neuroprotection and regeneration, that may be unique abducens
575 motoneuron responses to injury, are interesting avenues for future enquiry raised by the
576 present results.

57757

7

578 VEGF upregulates KCC2 levels in axotomized abducens motoneurons

579 Although VEGF was initially discovered by its action on blood vessels, from an
580 evolutionary point of view it emerged earlier as a neurotrophic factor, since it is essential
581 for the development of the nervous system in invertebrates lacking a vascular system or
582 having a rudimentary vasculature (Zacchigna et al. 2008). Nowadays, it is accepted that
583 VEGF is neuroprotective (Silva-Hucha et al. 2021). Our results show that exogenous
584 VEGF upregulated KCC2 in axotomized abducens motoneurons, and that this correlated
585 with increased efficiency of inhibitory signals in these motoneurons. To our knowledge,

586 this is the first time that KCC2 expression has been related to VEGF, however, the related
587 KCC3 was shown regulated by VEGF during its initial characterization (Hiki et al. 1999).

588 KCC2 transcription is promoted by Egr transcriptional factors downstream of the
589 rat sarcoma MAP kinase (Ras/MAPK) pathway (Ludwig et al. 2011) and several
590 neurotrophic factors converge in this pathway, including BDNF-TrkB and VEGF-
591 VEGFR2. KCC2 transcriptional regulation by BDNF has been found to be context
592 dependent. Thus, during development BDNF upregulates KCC2 and is involved in the
593 switch of depolarizing to hyperpolarizing actions of GABA (Aguado et al. 2003; Ludwig
594 et al. 2011). On the other hand, increases in local BDNF after injury in the adult frequently
595 downregulate KCC2 in many neurons (Rivera et al. 2002, 2004; Miletic and Miletic 2008;
596 Boulenguez et al. 2010), and effects are dependent on the signaling pathway selected
597 downstream of TrkB (Rivera et al. 2004). In adult neurons, KCC2 transcription is
598 downregulated by PLC γ 1 or Shc/FRS-2 signaling and upregulated by PI3K and
599 Ras/MAPK (Rivera et al. 2004). VEGF-VEGFR2 strongly activates PI3K and
600 Ras/MAPK cascades, while having limited effects on PLC γ 1 or Shc/FRS-2 pathways.

601 In addition to transcriptional regulation, posttranslational dephosphorylation at
602 specific KCC2 residues causes internalization (Lee et al. 2011; Bos et al. 2013). BDNF
603 activation of Shc/FRS-2 results in degradation of internalized KCC2 reducing membrane
604 levels. We previously showed that KCC2 removal from axotomized spinal motoneurons
605 is secondary to reduced *kcc2* mRNA expression independent of BDNF/TrkB, and KCC2
606 recovery occurred only after motoneurons reinnervated muscle (Akhter et al. 2019).
607 Likewise, muscle reinnervation restores KCC2 in axotomized facial (Kim et al. 2018) and
608 hypoglossal motoneurons (Tatetsu et al. 2012). Muscles express VEGF, where it mediates
609 hypoxia-induced angiogenesis during exercise and physiological adaptations (Gustafsson
610 2011; Hoier and Hellsten 2014). VEGF is expressed in the lateral rectus muscle, and

611 abducens motoneurons and their axons in the muscle are endowed with VEGF receptors
612 (Calvo et al. 2018; Silva-Hucha et al. 2020). It is thus possible that target-derived VEGF
613 acts as a retrograde factor regulating KCC2 in motoneurons. Axotomy did not
614 downregulate KCC2 in abducens motoneurons however, suggesting that additional
615 factors are necessary or that abducens motoneurons obtain VEGF from alternative
616 sources when disconnected from muscle. Nevertheless, exogenous application of VEGF
617 upregulated KCC2 expression above normal levels in injured abducens motoneurons.

61861
8

619 Functional correlates of VEGF upregulation of KCC2 in axotomized abducens
620 motoneurons

621 VEGF was shown to maintain normal physiological properties in axotomized
622 motoneurons with higher efficiency than other trophic factors (Calvo et al. 2018, 2020).
623 Axotomy changes abducens motoneuron firing because it alters both intrinsic properties
624 and function of synaptic inputs (Delgado-García et al. 1988; Calvo et al. 2018, 2020).
625 BDNF and NT-3 recover responses of axotomized abducens motoneurons to,
626 respectively, tonic and phasic inputs (Davis-López de Carrizosa et al. 2009), and NGF
627 recovers most properties and synaptic inputs, but above control values and with high
628 variability. Only VEGF consistently recovers all axotomy-induced alterations to control
629 levels (Calvo et al. 2018, 2020). In here, we reanalyzed our recordings to extract
630 specifically the gains of inhibitory off-rates and found a specific enhancement of
631 inhibitory inputs (i.e., k-off and r-off) by VEGF that was not previously reported.

632 VEGF restores to control values overall eye position and eye velocity sensitivities
633 (i.e., k and r) in axotomized motoneurons (Calvo et al. 2018). Herein, both sensitivities
634 were calculated separately during on *versus* off fixations (i.e., k-on and k-off) as well as
635 for on-directed *versus* off-directed saccades (i.e., r-on and r-off), being on the direction

636 of the lateral rectus muscle contraction and off the direction of relaxation. Axotomized
637 abducens motoneurons treated with VEGF exhibited higher k-off and r-off than control
638 motoneurons. In contrast, k-on and r-on were similar to control. This implied that VEGF
639 increased inhibitory synaptic input strength, in agreement with KCC2 upregulation. This
640 conclusion might also explain previous results on internuclear abducens neurons
641 axotomized at the level of medial longitudinal fascicle. This manipulation also decreases
642 excitatory and inhibitory inputs in these neurons, but when cut axons are provided with
643 an implant of neural progenitor cells, they retain inhibitory synapses and off-signals
644 similar to control values, whereas excitatory drive decreases normally (Morado-Díaz et
645 al. 2014). Neural progenitor cells express VEGF and it was suggested that this
646 neurotrophic factor could exert a direct influence in the efficacy of inhibitory signals
647 (Talaverón et al. 2013; Morado-Díaz et al. 2014). The data presented here confirm that
648 VEGF treatment upregulates KCC2 and can maintain or enhance inhibition in injured
649 neurons.

650 The causal link between VEGF and the upregulation of KCC2 opens the
651 possibility that the ionic balance is preserved when neurons access a source of trophic
652 factors that keep KCC2 expression at mature levels in motoneurons. The maintenance of
653 inhibitory chloride currents might also protect motoneurons from the deleterious action
654 of calcium-dependent excitotoxicity that makes motoneurons vulnerable in certain
655 pathologies such as amyotrophic lateral sclerosis (Fuchs et al. 2010).

65665

6

65765

7

658 **Author contributions:** The experiments were designed by FJA and AMP.
659 Immunocytochemistry and image analysis were carried out by PMC.
660 Electrophysiological experiments and analysis were carried out by PMC, AMP and RRC.
661 The manuscript was written by FJA, RRC and AMP. All authors have revised and accept
662 the final version of the manuscript.

663663

664 **Data availability.** The data supporting this study are available upon reasonable request
665 to the authors.

666666

667 **Conflict of interest.** The authors have no financial or non-financial interests to disclose.

668668

669 **Ethical approval** All animal procedures were performed at the University of Seville
670 (Spain) and in accordance with the guidelines of the European Union (2010/63/EU) and
671 Spanish legislation (R.D. 53/2013, BOE 34/11370-421) for the use and care of laboratory
672 animals. They were approved by the local ethics committee (Protocol #04/11/15/349).
673 Animal procedures also followed NIH guidelines and legislation in the US. No animal
674 experimentation was performed in the US for this project. Work at the US (Emory
675 University) consisted in immunocytochemical and morphological analyses of tissues
676 collected at University of Seville in Spain. All efforts were made to reduce the number of
677 animals used and their suffering during the present experiments and, in fact, some of the
678 material derives from the tissue bank of previously published studies (Calvo et al. 2018,
679 2020).

680

681

68

683 References

- 684 Aguado F, Carmona MA, Pozas E, Aguiló A, Martínez-Guijarro FJ, Alcantara S, Borrell
685 V, Yuste R, Ibañez CF, Soriano E (2003) BDNF regulates spontaneous correlated
686 activity at early developmental stages by increasing synaptogenesis and
687 expression of the K⁺/Cl⁻ co-transporter KCC2 . *Development* 130:1267-1280.
688 <https://doi.org/10.1242/dev.00351>
- 689 Akhter ET, Griffith RW, English AW, Alvarez FJ (2019) Removal of the potassium
690 chloride co-transporter from the somatodendritic membrane of axotomized
691 motoneurons is independent of BDNF/TrkB signaling but is controlled by
692 neuromuscular innervation. *eNeuro* 6:5. [https://doi.org/10.1523/eneuro.0172-](https://doi.org/10.1523/eneuro.0172-19.2019)
693 19.2019
- 694 Akita T, Fukuda A (2020) Intracellular Cl⁻ dysregulation causing and caused by
695 pathogenic neuronal activity. *Pflugers Arch* 472:977-987.
696 <https://doi.org/10.1007/s00424-020-02375-4>
- 697 Alvarez FJ, Rotterman TM, Akhter ET, Lane AR, English AW, Cope TC (2020)
698 Synaptic plasticity on motoneurons after axotomy: a necessary change in
699 paradigm. *Front Mol Neurosci* 13:68. <https://doi.org/10.3389/fnmol.2020.00068>
- 700 Azzouz M, Ralph GS, Storkebaum E, Walmsley LE, Mitrophanous KA, Kingsman SM,
701 Carmeliet P, Mazarakis ND (2004) VEGF delivery with retrogradely transported
702 lentivector prolongs survival in a mouse ALS model. *Nature* 429:413-417.
703 <https://doi.org/10.1038/nature02544>
- 704 Ben-Ari Y (2014) The GABA excitatory/inhibitory developmental sequence: a personal
705 journey. *Neuroscience* 279:187-219. [https://doi.org/10.1016/j.neuroscience.](https://doi.org/10.1016/j.neuroscience.2014.08.001)
706 2014.08.001
707

708 Benítez-Temiño B, Davis-López de Carrizosa MA, Morcuende S, Matarredona ER, de la
709 Cruz RR, Pastor AM (2016) Functional Diversity of Neurotrophin Actions on the
710 Oculomotor System. *Int J Mol Sci* 17:2016.
711 <https://doi.org/10.3390/ijms17122016>

712 Beverungen H, Klaszky SC, Klaszky M, Côté MP (2020) Rehabilitation decreases
713 spasticity by restoring chloride homeostasis through the brain-derived
714 neurotrophic factor-KCC2 pathway after spinal cord injury. *J Neurotrauma*
715 37:846-859. <https://doi.org/10.1089/neu.2019.6526>

716 Bilchak JN, Yeakle K, Caron G, Malloy D, Côté MP (2021) Enhancing KCC2 activity
717 decreases hyperreflexia and spasticity after chronic spinal cord injury. *Exp Neurol*
718 338:113605. <https://doi.org/10.1016/j.expneurol.2021.113605>

719 Bos R, Sadlaoud K, Boulenguez P, Buttigieg D, Liabeuf S, Brocard C, Haase G, Bras H,
720 Vinay L (2013) Activation of 5-HT_{2A} receptors upregulates the function of the
721 neuronal K-Cl cotransporter KCC2. *Proc Natl Acad Sci U S A* 110:348-
722 353. <https://doi.org/10.1073/pnas.1213680110>

723 Boulenguez P, Liabeuf S, Bos R, Bras H, Jean-Xavier C, Cécile Brocard C, Stil
724 A, Darbon P, Cattaert D, Delpire E, Marsala M, Vinay L (2010) Down-regulation
725 of the potassium-chloride cotransporter KCC2 contributes to spasticity after
726 spinal cord injury. *Nat Med* 16:302-307. <https://doi.org/10.1038/nm.2107>

727 Calvo PM, de la Cruz RR, Pastor AM (2018) Synaptic loss and firing alterations in
728 axotomized motoneurons are restored by vascular endothelial growth factor
729 (VEGF) and VEGF-B. *Exp Neurol* 304:67-81.
730 <https://doi.org/10.1016/j.expneurol.2018.03.004>

731 Calvo PM, de la Cruz RR, Pastor AM (2020) A single intraventricular injection of VEGF
732 leads to long-term neurotrophic effects in axotomized motoneurons. *eNeuro*7:3.
733 <https://doi.org/10.1523/eneuro.0467-19.2020>

734 Chamma I, Chevy Q, Poncer JC, Lévi S (2012) Role of the neuronal K-Cl co-transporter
735 KCC2 in inhibitory and excitatory neurotransmission. *Front Cell Neurosci* 6:5.
736 <https://doi.org/10.3389/fncel.2012.00005>

737 Côme E, Heubl M, Schwartz EJ, Poncer JC, Lévi S (2019) Reciprocal regulation
738 of KCC2 trafficking and synaptic activity. *Front Cell Neurosci* 13:48.
739 <https://doi.org/10.3389/fncel.2019.00048>

740 Cramer SW, Baggott C, Cain J, Tilghman J, Allcock B, Miranpuri G, Rajpal S, Sun D,
741 Resnick D (2008) The role of cation-dependent chloride transporters in
742 neuropathic pain following spinal cord injury. *Mol Pain* 4:36.
743 <https://doi.org/10.1186/1744-8069-4-36>

744 Davis-López de Carrizosa MA, Morado-Díaz CJ, Tena JJ, Benítez-Temiño B, Pecero
745 ML, Morcuende SR, de la Cruz RR, Pastor AM (2009) Complementary actions
746 of BDNF and neurotrophin-3 on the firing patterns and synaptic composition of
747 motoneurons. *J Neurosci* 29:575-587. [https://doi.org/10.1523/jneurosci.5312-](https://doi.org/10.1523/jneurosci.5312-08.2009)
748 [08.2009](https://doi.org/10.1523/jneurosci.5312-08.2009)

749 Davis-López de Carrizosa MA, Morado-Díaz CJ, Morcuende S, de la Cruz RR, Pastor
750 AM (2010) Nerve growth factor regulates the firing patterns and synaptic
751 composition of motoneurons. *J Neurosci* 30:8308-8319.
752 <https://doi.org/10.1523/jneurosci.0719-10.2010>

753 Davis-López de Carrizosa MA, Morado-Díaz CJ, Miller JM, de la Cruz RR, Pastor AM
754 (2011) Dual encoding of muscle tension and eye position by abducens
755 motoneurons. *J Neurosci* 31:2271-2279. [https://doi.org/10.1523/jneurosci.5416-](https://doi.org/10.1523/jneurosci.5416-10.2011)
756 [10.2011](https://doi.org/10.1523/jneurosci.5416-10.2011)

757 Davis-López de Carrizosa MA, Tena JJ, Benítez-Temiño B, Morado-Díaz CJ, Pastor
758 AM, de la Cruz RR (2008) A chronically implantable device for the controlled
759 delivery of substances, and stimulation and recording of activity in severed

760 nerves. *J Neurosci Methods* 167:302-309. <https://doi.org/10.1016/>
761 [j.jneumeth.2007.08.021](https://doi.org/10.1016/j.jneumeth.2007.08.021)

762 de la Cruz RR, Pastor AM, Martínez-Guijarro FJ, López-García C, Delgado-García JM
763 (1998) Localization of parvalbumin, calretinin, and calbindin D-28k in identified
764 extraocular motoneurons and internuclear neurons of the cat. *J Comp Neurol*
765 390:377-391. [https://doi.org/10.1002/\(sici\)1096-](https://doi.org/10.1002/(sici)1096-9861(19980119)390:3%3C377::aid-cne6%3E3.0.co;2-z)
766 [9861\(19980119\)390:3%3C377::aid-cne6%3E3.0.co;2-z](https://doi.org/10.1002/(sici)1096-9861(19980119)390:3%3C377::aid-cne6%3E3.0.co;2-z)

767 Delgado-García JM, del Pozo F, Baker R (1986a) Behavior of neurons in the abducens
768 nucleus of the alert cat-I. Motoneurons. *Neuroscience* 17:929-952.
769 [https://doi.org/10.1016/0306-4522\(86\)90072-2](https://doi.org/10.1016/0306-4522(86)90072-2)

770 Delgado-García JM, del Pozo F, Baker R (1986b) Behavior of neurons in the abducens
771 nucleus of the alert cat-II. Internuclear neurons. *Neuroscience* 17:953-973.
772 [https://doi.org/10.1016/0306-4522\(86\)90073-4](https://doi.org/10.1016/0306-4522(86)90073-4)

773 Delgado-García JM, Del Pozo F, Spencer RF, Baker R (1988) Behavior of neurons in the
774 abducens nucleus of the alert cat-III. Axotomized motoneurons. *Neuroscience*
775 24:143-160. [https://doi.org/10.1016/0306-4522\(88\)90319-3](https://doi.org/10.1016/0306-4522(88)90319-3)

776 Dukkupati SS, Chihi A, Wang Y, Elbasiouny SM. (2017) Experimental Design and Data
777 Analysis Issues Contribute to Inconsistent Results of C-Bouton Changes in
778 Amyotrophic Lateral Sclerosis. *eNeuro*. 4(1): ENEURO.0281-16.2016.
779 <https://doi.org/10.1523/ENEURO.0281-16.2016>

780 Escudero M, de la Cruz RR, Delgado-García JM (1992) A physiological study of
781 vestibular and prepositus hypoglossi neurones projecting to the abducens nucleus
782 in the alert cat. *J Physiol* 458:539-560.
783 <https://doi.org/10.1113/jphysiol.1992.sp019433>

784 Escudero M, Delgado-García JM (1988) Behavior of reticular, vestibular and prepositus
785 neurons terminating in the abducens nucleus of the alert cat. *Exp Brain Res*

786 71:218-222. <https://doi.org/10.1007/bf00247538>

787 Fuchs A, Ringer C, Bilkei-Gorzo A, Weihe E, Roeper J, Schütz B (2010).
788 Downregulation of the potassium chloride cotransporter KCC2 in vulnerable
789 motoneurons in the SOD1-G93A mouse model of amyotrophic lateral sclerosis. *J*
790 *Neuropathol Exp Neurol* 10:1057-1070.
791 <https://doi.org/10.1097/nen.0b013e3181f4dcef>

792 Gagnon M, Bergeron MJ, Lavertu G, Castonguay A, Tripathy S, Bonin RP, Perez-
793 Sanchez J, Boudreau D, Wang B, Dumas L, Valade I, Bachand K, Jacob-Wagner
794 M, Tardif C, Kianicka I, Isenring P, Attardo G, Coull JA, De Koninck Y (2013)
795 Chloride extrusion enhancers as novel therapeutics for neurological diseases. *Nat*
796 *Med* 19:1524-1528. <https://doi.org/10.1038/nm.3356>

797 Gey M, Wanner R, Schilling C, Pedro MT, Sinske D, Knöll B (2016) Atf3 mutant mice
798 show reduced axon regeneration and impaired regeneration-associated gene
799 induction after peripheral nerve injury. *Open Biol* 6:160091.
800 <https://doi.org/10.1098/rsob.160091>

801 Gustafsson T (2011) Vascular remodelling in human skeletal muscle. *Biochem Soc Trans*
802 39:1628-1632. <https://doi.org/10.1042/bst20110720>

803 Hiki K, D'Andrea RJ, Furze J, Crawford J, Woollatt E, Sutherland GR, Vadas MA,
804 Gamble JR (1999) Cloning, characterization, and chromosomal location of a novel
805 human K⁺-Cl⁻ cotransporter. *J Biol Chem* 274:10661-106617- Hoier B, Hellsten
806 Y (2014) Exercise-induced capillary growth in human skeletal muscle and the
807 dynamics of VEGF. *Microcirculation* 21:301-314.
808 <https://doi.org/10.1074/jbc.274.15.10661>

809 Ho J, Tumkaya T, Aryal S, Choi H, Claridge-Chang A. (2019) Moving beyond P values:
810 data analysis with estimation graphics. *Nat Methods*. 16:565-566.
811 <https://doi.org/10.1038/s41592-019-0470-3>

812 Holland SD, Ramer LM, McMahon SB, Denk F, Ramer MS (2019) An ATF3-CreERT2
813 Knock-In Mouse for Axotomy-Induced Genetic Editing: Proof of Principle.
814 eNeuro 6:2. <https://doi.org/10.1523/eneuro.0025-19.2019>

815 Kahle KT, Khanna A, Clapham DE, Woolf CJ (2014) Therapeutic restoration of spinal
816 inhibition via druggable enhancement of potassium-chloride cotransporter KCC2-
817 mediated chloride extrusion in peripheral neuropathic pain. JAMA Neurol
818 71:640-645. <https://doi.org/10.1001/jamaneurol.2014.21>

819 Kaila K, Price TJ, Payne JA, Puskarjov M, Voipio J (2014) Cation-chloride
820 cotransporters in neuronal development, plasticity and disease. Nat Rev Neurosci
821 15:637-654. <https://doi.org/10.1038/nrn3819>

822 Kim J, Kobayashi S, Shimizu-Okabe C, Okabe A, Moon C, Shin T, Takayama C.J (2018)
823 Changes in the expression and localization of signaling molecules in
824 mouse facial motor neurons during regeneration of facial nerves. Chem
825 Neuroanat 88:13-21. <https://doi.org/10.1016/j.jchemneu.2017.11.002>

826 Lee HH, Deeb TZ, Walker JA, Davies PA, Moss SJ (2011) NMDA receptor activity
827 downregulates KCC2 resulting in depolarizing GABAA receptor-mediated
828 currents. Nat Neurosci 14:736-743. <https://doi.org/10.1038/nn.2806>

829 Lee-Hotta S, Uchiyama Y, Kametaka S (2019) Role of the BDNF-TrkB pathway in
830 KCC2 regulation and rehabilitation following neuronal injury: A mini review.
831 Neurochem Int 128:32-38.

832 Lorenzo LE, Godin AG, Ferrini F, Bachand K, Plasencia-Fernandez I, Labrecque S,
833 Girard AA, Boudreau D, Kianicka I, Gagnon M, Doyon N, Ribeiro-da-Silva A,
834 De Koninck Y (2020) Enhancing neuronal chloride extrusion rescues $\alpha 2/\alpha 3$
835 GABAA-mediated analgesia in neuropathic pain. Nat Commun 11:869.
836 <https://doi.org/10.1038/s41467-019-14154-6>

837 Ludwig A, Uvarov P, Soni S, Thomas-Crusells J, Airaksinen MS, Rivera CJ (2011) Early
838 growth response 4 mediates BDNF induction of potassium chloride cotransporter
839 2 transcription. *J Neurosci* 31:644-649. [https://doi.org/10.1523/jneurosci.2006-](https://doi.org/10.1523/jneurosci.2006-10.2011)
840 10.2011

841 Markkanen M, Karhunen T, Llano O, Ludwig A, Rivera C, Uvarov P, Airaksinen MS
842 (2014) Distribution of neuronal KCC2a and KCC2b isoforms in mouse CNS. *J*
843 *Comp Neurol* 522:1897-1914. <https://doi.org/10.1002/cne.23510>

844 Medina I, Friedel P, Rivera C, Kahle KT, Kourdougli N, Uvarov P, Pellegrino C (2014)
845 Current view on the functional regulation of the neuronal K(+)-Cl(-)
846 cotransporter KCC2. *Front Cell Neurosci* 8:27.
847 <https://doi.org/10.3389/fncel.2014.00027>

848 Miletic G, Miletic V (2008) Loose ligation of the sciatic nerve is associated with TrkB
849 receptor-dependent decreases in KCC2 protein levels in the ipsilateral spinal
850 dorsal horn. *Pain* 137:532-539. <https://doi.org/10.1016/j.pain.2007.10.016>

851 Moore YE, Deeb TZ, Chadchankar H, Brandon NJ, Moss SJ (2018) Potentiating KCC2
852 activity is sufficient to limit the onset and severity of seizures. *Proc Natl Acad Sci*
853 *U S A* 115:10166-10171. <https://doi.org/10.1073/pnas.1810134115>

854 Morado-Díaz CJ, Matarredona ER, Morcuende S, Talaverón R, Davis-López de
855 Carrizosa MA, de la Cruz RR, Pastor AM (2014) Neural progenitor cell implants
856 in the lesioned medial longitudinal fascicle of adult cats regulate synaptic
857 composition and firing properties of abducens internuclear neurons. *J Neurosci*
858 34:7007-7017. <https://doi.org/10.1523/jneurosci.4231-13.2014>

859 Nabekura J, Ueno T, Okabe A, Furuta A, Iwaki T, Shimizu-Okabe C, Fukuda A, Akaike
860 N (2002) Reduction of KCC2 expression and GABA_A receptor-mediated
861 excitation after in vivo axonal injury. *J Neurosci* 22:4412-
862 4417. <https://doi.org/10.1523/jneurosci.22-11-04412.2002>

863 Oosthuysen B, Moons L, Storkebaum E et al. (2001) Deletion of the hypoxia-response
864 element in the vascular endothelial growth factor promoter causes motor neuron
865 degeneration. *Nat Genet* 28:131-138. <https://doi.org/10.1038/88842>

866 Palma E, Amici M, Sobrero F, Spinelli G, Di Angelantonio S, Ragozzino D, Mascia
867 A, Scoppetta C, Esposito V, Miledi R, Eusebi F (2006) Anomalous levels of Cl-
868 transporters in the hippocampal subiculum from temporal lobe epilepsy patients
869 make GABA excitatory. *Proc Natl Acad Sci U S A* 103:8465-8468.
870 <https://doi.org/10.1073/pnas.0602979103>

871 Papp E, Rivera C, Kaila K, Freund TF (2008) Relationship between neuronal
872 vulnerability and potassium-chloride cotransporter 2 immunoreactivity in
873 hippocampus following transient forebrain ischemia. *Neuroscience* 154:677-689.
874 <https://doi.org/10.1016/j.neuroscience.2008.03.072>

875 Patodia S, Raivich G (2012) Role of transcription factors in peripheral nerve regeneration.
876 *Front Mol Neurosci* 5:8. <https://doi.org/10.3389/fnmol.2012.00008>

877 Payne JA, Rivera C, Voipio J, Kaila K (2003) Cation-chloride co-transporters in neuronal
878 communication, development and trauma. *Trends Neurosci* 26:199-206.
879 [https://doi.org/10.1016/s0166-2236\(03\)00068-7](https://doi.org/10.1016/s0166-2236(03)00068-7)

880 Payne JA, Stevenson TJ, Donaldson LF (1996) Molecular characterization of a putative
881 K-Cl cotransporter in rat brain. A neuronal-specific isoform. *J Biol Chem*
882 271:16245-16252. <https://doi.org/10.1074/jbc.271.27.16245>

883 Peerboom C, Wierenga CJ (2021) The postnatal GABA shift: A developmental
884 perspective. *Neurosci Biobehav Rev* 124:179-192.
885 <https://doi.org/10.1016/j.neubiorev.2021.01.024>

886 Pozzi D, Rasile M, Corradini I, Matteoli M (2020) Environmental regulation of the
887 chloride transporter KCC2: switching inflammation off to switch the GABA on?
888 *Transl Psychiatry* 10:349. <https://doi.org/10.1038/s41398-020-01027-6>

889 Rivera C, Li H, Thomas-Crusells J, Lahtinen H, Viitanen T, Nanobashvili A, Kokaia Z,
890 Airaksinen MS, Voipio J, Kaila K, Saarma M (2002) BDNF-induced TrkB
891 activation down-regulates the K⁺-Cl⁻ cotransporter KCC2 and impairs neuronal
892 Cl⁻ extrusion. *J Cell Biol* 159:747-752. <https://doi.org/10.1083/jcb.200209011>

893 Rivera C, Voipio J, Payne JA, Ruusuvuori E, Lahtinen H, Lamsa K, Pirvola U, Saarma
894 M, Kaila K (1999) The K⁺/Cl⁻ co-transporter KCC2 renders GABA
895 hyperpolarizing during neuronal maturation. *Nature* 397:251-255.
896 <https://doi.org/10.1038/16697>

897 Rivera C, Voipio J, Thomas-Crusells J, Li H, Emri Z, Sipilä S, Payne JA, Minichiello L,
898 Saarma M, Kaila K (2004) Mechanism of activity-dependent downregulation of
899 the neuron-specific K-Cl cotransporter KCC2. *J Neurosci* 24:4683-
900 4691. <https://doi.org/10.1523/jneurosci.5265-03.2004>

901 Seiffers R, Mills CD, Woolf CJ (2007) ATF3 increases the intrinsic growth state of DRG
902 neurons to enhance peripheral nerve regeneration. *J Neurosci* 27:7911-20.
903 <https://doi.org/10.1523/jneurosci.5313-06.2007>

904 Silva-Hucha S, Carrero-Rojas G, Fernández de Sevilla ME, Benítez-Temiño B, Davis-
905 López de Carrizosa MA, Pastor AM, Morcuende S (2020) Sources and lesion-
906 induced changes of VEGF expression in brainstem motoneurons. *Brain Struct*
907 *Funct* 225:1033-1053. <https://doi.org/10.1007/s00429-020-02057-y>

908 Talaverón R, Matarredona ER, de la Cruz RR, Pastor AM (2013)
909 Neural progenitor cell implants modulate vascular endothelial growth factor and
910 brain-derived neurotrophic factor expression in rat axotomized neurons. *PLoS*
911 *One* 8:e54519. <https://doi.org/10.1371/journal.pone.0054519>

912 Tatetsu M, Kim J, Kina S, Sunakawa H, Takayama C (2012) GABA/glycine signaling
913 during degeneration and regeneration of mouse hypoglossal nerves. *Brain Res*
914 1446:22-33. <https://doi.org/10.1016/j.brainres.2012.01.048>

915 Tovar-y-Romo LB, Zepeda A, Tapia R (2007) Vascular endothelial growth factor
916 prevents paralysis and motoneuron death in a rat model of excitotoxic spinal cord
917 neurodegeneration. *J Neuropathol Exp Neurol* 66:913-922.
918 <https://doi.org/10.1097/nen.0b013e3181567c16>

919 Toyoda H, Ohno K, Yamada J, Ikeda M, Okabe A, Sato K, Hashimoto K, Fukuda A (2003)
920 Induction of NMDA and GABAA receptor-mediated Ca²⁺ oscillations with
921 KCC2 mRNA downregulation in injured facial motoneurons. *J Neurophysiol*
922 89:1353-1362. <https://doi.org/10.1152/jn.00721.2002>

923 Tsujino H, Kondo E, Fukuoka T, Dai Y, Tokunaga A, Miki K, Yonenobu K, Ochi T,
924 Noguchi K (2000) Activating transcription factor 3 (ATF3) induction by axotomy
925 in sensory and motoneurons: a novel neuronal marker of nerve injury. *Mol Cell*
926 *Neurosci* 15:170-182. <https://doi.org/10.1006/mcne.1999.0814>

927 Uvarov P, Ludwig A, Markkanen M, Pruunsild P, Kaila K, Delpire E, Timmusk T, Rivera
928 C, Airaksinen MS (2007) A novel N-terminal isoform of the neuron-specific K-
929 Cl cotransporter KCC2. *J Biol Chem* 282:30570-30576.
930 <https://doi.org/10.1074/jbc.m705095200>

931 Woo N-S, Lu J, England R, McClellan R, Dufour S, Mount DB, Deutch AY, Lovinger
932 DM, Delpire E (2002) Hyperexcitability and epilepsy associated with disruption
933 of the mouse neuronal-specific K-Cl cotransporter gene. *Hippocampus* 12:258-
934 268. <https://doi.org/10.1002/hipo.10014>

935 Zacchigna S, Lambrechts D, Carmeliet P (2008) Neurovascular signaling defects in
936 neurodegeneration. *Nat Rev Neurosci* 9:169-
937 181. <https://doi.org/10.1038/nrn2336>

938 Zhu L, Polley N, Mathews GC, Delpire E (2008) NKCC1 and KCC2 prevent
939 hyperexcitability in the mouse hippocampus. *Epilepsy Res* 79:201-212.
940 <https://doi.org/10.1016/j.eplepsyres.2008.02.005>

941 FIGURE LEGENDS

942 **Fig. 1** Presence of KCC2 and KCC2 isoforms in the cat abducens nucleus. **A-C** Low
943 magnification confocal images (2D projection of a 50 μm confocal stack) of the abducens
944 nucleus showing motoneurons labeled with choline acetyltransferase (ChAT) (**A**, green),
945 abducens internuclear neurons labeled with calretinin (CR) (**B**, cyan) and pan-KCC2
946 (pKCC2 **C**, red) (dashed line delimits the facial nerve genu for anatomical orientation).
947 **D** High magnification single plane confocal image showing double immunofluorescence
948 for ChAT and pKCC2 in abducens motoneurons. **E** Same as **D** for an abducens
949 internuclear neuron. **F-I** Single plane confocal images showing triple
950 immunofluorescence against ChAT (green in **F** and **H**), KCC2b (red in **F**) and KCC2a
951 (blue in **H**) in abducens motoneurons. KCC2b and KCC2a are shown in black and white
952 for better discrimination in **G** and **I**. KCC2b labeling of somata and dendrites is similar
953 to pKCC2. KCC2a labeling was intracellular. Scale bars = 150 μm in **C** for **A-C**; 15 μm
954 in **E** for **D-E**; 30 μm in **I** for **F-I**

955955

956 **Fig. 2** Changes in KCC2 levels induced by axotomy and VEGF administration in cat
957 abducens motoneurons. **A, D, G** Confocal images showing abducens motoneurons
958 identified by ChAT immunolabeling in the three experimental situations: control (**A**),
959 axotomy (**D**), and axotomy plus VEGF administration (**G**). **B, E, H** Same regions as in
960 **A, D** and **G**, respectively, but showing the red channel with pan(p)KCC2
961 immunostaining. **C, F, I** Merge of ChAT and pKCC2 immunolabelings. KCC2
962 immunolabels the surface of cell bodies and proximal dendrites of all motoneurons
963 independent of the experimental condition. Asterisks in **D-I** point to ChAT-
964 immunonegative abducens internuclear neurons. **J** Quantitative comparison of pKCC2
965 immunofluorescence in abducens motoneurons in control, axotomy and axotomy +

966 VEGF. No significant (n.s.) differences were observed between control and axotomized
967 abducens motoneurons, whereas axotomized motoneurons treated with VEGF showed a
968 significantly (asterisk) higher pKCC2 level than control ($p = 0.017$) and axotomized ($p =$
969 0.004) motoneurons, respectively; one-way ANOVA test followed by Holm-Sidak
970 method; $n = 122, 71$ and 72 motoneurons analyzed in control, axotomized and axotomized
971 + VEGF-treated conditions, respectively. **K** Swarm dot plots of raw data (individual
972 motoneurons) and differences for comparisons against the shared control shown in
973 Cumming estimation plots. The distribution of differences obtained from bootstrap
974 resampling are shown with the mean difference depicted as a dot and the 95% confidence
975 interval indicated by the ends of the vertical error bars. No statistically significant
976 difference was found when comparing axotomy to control, but a 21% significant increase
977 was detected in motoneurons treated with VEGF (two-sided permutation t-test $p =$
978 0.0216). **L** Quantitative analyses of pKCC2 and KCC2b in abducens motoneuron in
979 control and axotomy. No significant differences (two-way ANOVA) were found
980 according to the type of KCC2 immunoreactivity (pKCC2 or KCC2b; $p = 0.089$) or
981 experimental condition (control or axotomized; $p = 0.166$). Scale bar = $40 \mu\text{m}$ in **I** for **A-**
982 **I**

98398
3

984 **Fig. 3.** KCC2 changes induced by axotomy in cat spinal motoneurons. **A-H** High
985 magnification single plane confocal images of spinal motoneurons immunostained
986 against ChAT, pKCC2 and ATF3. **A-D** corresponds to a control motoneuron and **E-H** to
987 a motoneuron axotomized 21 days previously. Individual immunoreactivities are
988 presented in isolation and the merged (**D, H**) as indicated in the figure. Axotomized
989 motoneurons expressed ATF3 in the nucleus (arrow in **G**) and decreased ChAT
990 immunoreactivity (**E**). They also lacked surface pKCC2 immunoreactivity in the cell

991 body and proximal dendrite surfaces (**F**). **I** Axotomized spinal motoneuron
992 immunolabeled for ChAT and ATF3. **J** KCC2b immunofluorescence of the same
993 axotomized motoneuron as in **I** illustrating lack of KCC2b labeling in its somatic
994 membrane. **K** Merge image of **I** and **J**. **L** Comparison of pKCC2 immunofluorescence
995 between control and axotomized spinal motoneurons. Axotomized spinal motoneurons
996 showed a significantly (asterisk) lower level of pKCC2 than control spinal motoneurons
997 (t-test, $p \leq 0.001$; $n = 96$ and 101 control and axotomized motoneurons, respectively). **M**
998 Swarm dot plots of raw data (individual motoneurons) and differences between control
999 (blue) and axotomy (yellow) shown in Cumming estimation plots. The distribution of
100 differences obtained from bootstrap resampling are shown with the mean difference
0
100 depicted as a dot and the 95% confidence interval indicated by the ends of the vertical
1 error bars. A 70% significant decrease was detected in axotomized spinal motoneurons
2
100 (two-sided permutation t-test $p < 0.001$). **N** Bar chart illustrating the results of a two-way
3
100 ANOVA test and Holm-Sidak method comparing the following two factors: experimental
4
100 condition (control *versus* axotomy) and type of KCC2 immunoreactivity (pKCC *versus*
5
100 KCC2b). Data were gathered from one cat stained in serial sections with pKCC2 and
6
100 KCC2b (control, $n = 29$ and 26 motoneurons; axotomy, $n = 33$ and 27 motoneurons for
7
100 pKCC2 and KCC2b, respectively). Two-way ANOVA detected significant differences in
8
100 control *vs.* axotomized motoneurons (asterisk, $p < 0.001$), but no difference between
9
101 pKCC2 and KCC2b ($p = 0.099$, *n.s.*), or the interaction between axotomy and type of
0
101 immunoreactivity ($p = 0.334$). *Post-hoc* Holm-Sidak pair-wise comparisons revealed
1
101 significant difference between control and injured motoneuron for pKCC2 and KCC2b
2
101 (#, $p < 0.001$ for both). **O**, Swarm dot plots of raw data (individual motoneurons) and
3

101 differences between pKCC2 in control (blue), KCC2b in control (yellow) and pKCC2
4
101 after axotomy (green) and KCC2b after axotomy (red) all shown in Cumming estimation
5
101 plots. The distribution of differences obtained from bootstrap resampling are shown with
6

101 the mean difference depicted as a dot and the 95% confidence interval indicated by the
 7
 101 ends of the vertical error bars. No significant differences were found between KCC2b and
 8
 101 pKCC2 in control motoneurons. Axotomized motoneurons showed a 70% significant
 9
 102 decrease compared to their respective antibody matched controls (two-sided permutation
 0
 102 t-test $p < 0.001$ in both comparisons). Scale bars = 30 μm in **H** for **A-H**; 20 μm in **K** for
 1
 102 **I-K**
 2
 102
 3
 102 **Fig. 4** KCC2 immunoreactivity in brainstem oculomotor, trochlear, abducens and facial
 4
 102 motoneurons, in control and after axotomy, in the rat. **A, C, E, G** Confocal images of
 5
 102 double immunofluorescence against ChAT (green) and pKCC2 (red) in control
 6
 102 oculomotor (**A**), trochlear (**C**), abducens (**E**) and facial (**G**) motoneurons. **B, D, F, H**
 7
 102 Confocal images of triple immunofluorescence against ChAT (green), KCC2 (red) and
 8
 102 ATF3 (white) in the same brainstem nuclei, but after axotomy. Axotomized oculomotor,
 9
 103 trochlear and facial motoneurons showed a marked reduction in pKCC2 and ChAT. ATF3
 0
 103 is a general marker of axotomized motoneurons and labels the cell nucleus, as can be
 1
 103 observed in axotomized oculomotor (**B**), trochlear (**D**) and facial (**H**) motoneurons (some
 2
 103 examples are indicated by white arrows). However, in axotomized abducens motoneurons
 3
 103 (**F**), immunostaining for pKCC2 and ChAT showed a similar appearance to control (**E**),
 4
 103 and ATF3 labeling was absent. **I** Quantification of KCC2 immunofluorescence in the four
 5
 103 nuclei (oculomotor, trochlear, abducens and facial) and in the control and axotomy
 6
 103 situation. Asterisks indicate significant ($p < 0.001$) difference between control and
 7
 103 axotomized motoneurons within the same nucleus. Hashtag indicates significant
 8

103 difference ($p < 0.001$) between axotomized abducens motoneurons and the axotomized
9
104 motoneurons of the other three nuclei. Two-way ANOVA followed by Holm-Sidak
0
104 method ($n = 35, 36, 33$ and 39 for control and $n = 33, 35, 44$ and 42 for axotomized
1

104 motoneurons of the oculomotor, trochlear, abducens and facial nuclei, respectively. Data
2
104 in histograms represent mean \pm SEM. Depicted to the right are the Cumming plots of
3
104 estimated differences after bootstrap resampling with average difference indicated by a
4
104 dot and 95% CI limit of the distribution by the vertical bars. Oculomotor, trochlear and
5
104 facial motoneurons all showed significant reduction of 72%, 89% and 87% of the control
6
104 value, respectively (two-sided permutation t-test $p < 0.001$ for all comparisons). There
7
104 was no significant differences when comparing axotomized and control motoneurons in
8
104 the abducens nucleus. Scale bar = 30 μm in **H** for **A-H**
9

105
0

105 **Fig. 5** Procedure to calculate k-on, k-off, r-on and r-off in the discharge activity of
1
105 abducens motoneurons. In **A** and **C**, from top to bottom: eye position (EP, in degrees),
2
105 eye velocity (EV, in degrees/s) and firing rate (FR, in spikes/s) of a control abducens
3
105 motoneuron during spontaneous eye movements. The double arrow in **A** indicates
4
105 leftward (L) and rightward (R) eye movements. **B** FR and EP correlates by means of a
5
105 linear regression line whose slope represents the neuronal eye position sensitivity (k, in
6
105 spikes/s/degree; line in black). When eye fixations are separated between those occurring
7
105 after an on-directed saccade (arrows in **A** in the traces of EP and FR) and those after an
8
105 off-directed saccade (arrowheads in **A** in the traces of EP and FR), then the neuronal eye
9
106 position sensitivity can be calculated independently for on-fixations *versus* off-fixations,
0
106 thus obtaining the parameters k-on (in orange) and k-off (in red), respectively. **D** The
1
106 neuronal eye velocity sensitivity during saccades (r, in spikes/s/degree/s) is obtained as
2
106 the slope of the linear regression line between FR (previous subtraction of the EP
3

106 component, FR-k·EP) and EV (line in black). If the analysis is performed separating on-
4

106 directed saccades and their corresponding neuronal bursts in FR (arrows in **C** in the traces
5

106 of EV and FR) from off-directed saccades and their corresponding decreases in FR
6

106 (arrowheads in **C** in the traces of EV and FR), then r-on (in orange) and r-off (in red)
7

106 sensitivities, respectively, are obtained. Off-directed saccades accompanied by a cut-off
8

106 in FR (asterisks in **C**) were discarded from the calculation of r-off parameter
9

107
0

107 **Fig. 6** Quantitative analysis of neuronal sensitivities to eye position and velocity
1

107 depending on the on- or off-direction of the fixation or saccade. **A, B** Plots representing
2

107 neuronal eye position sensitivity during off-fixations (k-off, in **A**) and neuronal eye
3

107 velocity during off-saccades (r-off, in **B**) illustrated for the three experimental groups:
4

107 control, axotomy, and axotomy + VEGF. **C, D** Same as **A, B** but for k-on (**C**) and r-on
5

107 (**D**). The asterisks in **A, B** indicate significant difference ($p < 0.05$) in k-off (**A**) and r-off
6

107 (**B**) between the axotomized motoneurons treated with VEGF with respect to control and
7

107 axotomized untreated motoneurons. In **C, D** the asterisks indicate significant differences
8

107 ($p < 0.05$) between axotomy *versus* the other two groups (for **A-D**, one-way ANOVA test,
9

108 $p \leq 0.001$, followed by Dunn's method for all pairwise multiple comparisons). The
0

108 number of motoneurons analyzed in control, axotomy and axotomy + VEGF was 21, 17
1

108 and 18, respectively.
2